社団法人 情報処理学会　研究報告
IPSJ SIG Technical Report

2004－CVIM－144　(23)
2004／5／6

Illumination Color and Intrinsic Surface Properties - Physics-based Color Analyses from a Single Image -

Robby T. Tan　　Katsushi Ikeuchi

Department of Computer Science
The University of Tokyo
{robby,ki}@cvl.iis.u-tokyo.ac.jp

Abstract

A consistent color descriptor of an object is a significant requirement for many applications in computer vision. In the real world, unfortunately, the color appearances of objects are generally not consistent. It depends principally on two factors: illumination spectral power distribution (illumination color) and intrinsic surface properties. Consequently, to obtain objects' consistent color descriptors, we have to deal with those two factors. The former is commonly referred to as color constancy: a capability to estimate and discount the illumination color, while the latter is identical to the problem of recovering body color from highlights. This recovery is crucial because highlights emitted from opaque inhomogeneous objects can cause the surface colors to be inconsistent with regard to the change of viewing and illuminant directions.

We base our color constancy methods on analyzing highlights or specularities emitted from opaque inhomogeneous objects. We have successfully derived a linear correlation between image chromaticity and illumination chromaticity. This linear correlation is clearly described in inverse-intensity chromaticity space, a novel two-dimensional space we introduce. Through this space, we become able to effectively estimate illumination chromaticity (illumination color) from both uniformly colored surfaces and highly textured surfaces in a single integrated framework, thereby making our method significantly advanced over the existing methods. By knowing the illumination chromaticity, we can normalize the input image such that its illumination color becomes pure white. Meanwhile, for separating reflection components, we propose an approach that is based on an iterative framework and a specular-free image. The specular-free image is an image that is free from specularities yet has different body color from the input image. In general, the approach relies principally on image intensity and color.

All methods of color constancy and reflection-components separation proposed in this paper are analyzed based on physical phenomena of the real world, making the estimation more accurate, and have strong basics of analysis. In addition, all methods require only a single input image. This is not only practical, but also challenging in term of complexity.

1 Introduction

The color appearance of an object is not the object's actual color. Several factors, mainly illumination and object surface's intrinsic properties, play significant roles in determining the object color appearance. In our daily life, we can easily find the roles of illumination color in many occasions, for example, an outdoor scene under a clear sky will look redder in the evening than in the middle of the day, or an object will look greener if lit by a green lamp. However, although the color appearance of an object or a scene changes as a consequence of illumination change, we are still, at a certain level of accuracy, able to identify the actual color of the object or the scene. This capability is called color constancy. It is inherent in human perception and one of the important aspects of object recognition processes.

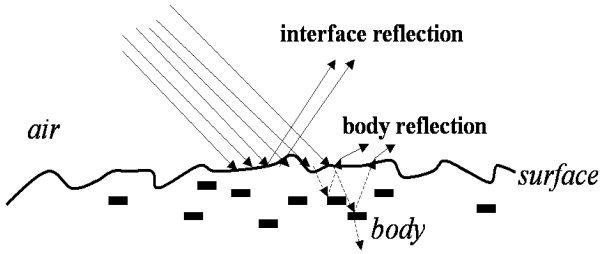

Figure 1: The mechanism of reflected light on inhomogeneous opaque surface

In machine vision, color constancy is also a crucial requirement for various applications, e.g., color-based object recognition, color reproduction, image retrieval, reflection components separation, image-based rendering, and so on. Unfortunately, up to now, the mechanism of human perception color constancy has not been well understood, making it impossible to apply it to machine vision. For decades, this has motivated researchers in machine vision to develop various color constancy algorithms, which do not necessarily correspond to human biological color constancy.

Generally, color constancy is defined as the capability to recover the actual color of an object. It implies that, although the illumination color changes, we can obtain a consistent color descriptor of the object. This consistency is the most fundamental aspect of color constancy. However, while it is correct for diffuse objects, the consistency is still partially correct for certain types of objects that exhibit highlights. In diffuse objects, if we have discounted the illumination color and obtained their actual color, we will have a consistent color descriptor even if either our viewing position or the illumination direction changes. On the contrary, for objects exhibiting highlights, although we have discounted the illumination color, the colors of certain patches of the objects are still inconsistent w.r.t. the change of viewing and illumination directions. The reason is, the locations of highlights, which are caused by the presence of specular reflection, are inconsistent w.r.t. the changes of viewing and illumination directions. As a consequence, color constancy alone is insufficient to acquire a consistent color descriptor of general types of objects. For this reason, in this paper, instead of dealing solely with illumination color, we also deal with object surface intrinsic properties.

Based on its reflection components, basically intrinsic surface properties can be divided into two components: diffuse (body) and specular (interface) reflections. Figure 1 shows a pictorial mechanism of reflected light rays. Once a bundle of light rays enters an inhomogeneous opaque surface, some of the rays will immediately reflect back into the air, while the remainder will penetrate the body of the object. Some of these penetrating light rays will go through the body; others will re-

flect back onto the surface and then into the air. The immediately reflected light rays are called *interface* or *specular* reflection, while those that have penetrated and then reflected back into the air are called *body* or *diffuse* reflection. Note that, besides those two reflections, physically there is another component called *specular spike* [3, 32]. However, since its presence is very minor in inhomogeneous object, we can ignore it. Thus, highlights emitted from inhomogeneous objects are the combination of diffuse and specular reflections. Unlike diffuse reflection, the location of specular reflection depends on viewing and illumination directions, causing its appearance to be inconsistent. On the contrary, diffuse reflection is independent from viewing position, and dependent only on illumination direction in term of its intensity magnitude. This means that the color descriptor of diffuse reflection, which is usually a normalized value, is independent of both viewing position and illumination directions. As a consequence, to be able to obtain a consistent color descriptor, we have to decompose or separate the reflection components and then acquire diffuse only reflection. Moreover, once we acquire diffuse only reflection, we become able to observe the body color beneath highlights.

Goals Considering the importance in various machine vision applications, therefore, the ultimate purpose of this paper is to describe how to extract the actual color of diffuse reflection components. Basically, two processes are required to achieve our purpose, namely, color constancy and reflection components separation. We base our color constancy methods on analyzing highlights or specularities emitted from opaque inhomogeneous objects. We have successfully derived a linear correlation between image chromaticity and illumination chromaticity. This linear correlation is clearly described in inverse-intensity chromaticity space, a novel two-dimensional space which we introduce. Through this space, we become able to effectively estimate illumination chromaticity (illumination color) from both uniformly colored surfaces and highly textured surfaces in a single integrated framework, thereby making our method significantly more advanced than the existing methods. Moreover, unlike the existing methods based on specularities, thanks to the linear correlation, we do not need to segment surface colors beneath the highlights. Meanwhile, for separating reflection components, we propose an approach based on intensity and color differences between highlights and diffuse reflections.

In general, the flow of our framework can be depicted in Figure 2. Top of the figure (2.a) shows an opaque inhomogeneous object lit by an incandescent lamp. By using our proposed color constancy method, we estimate the illumination color and then normalize the image, making the illumination color becomes pure-white as shown in Figure 2.b. Then, after normalizing the image, we decompose it into its reflection components. Figure 2.c-d shows the decomposition results: diffuse reflection component and specular reflection component, respectively. All approaches of color constancy and reflection-components separation in this paper are analyzed based on physical phenomena of the real world, making the computation more accurate and have strong basics of analysis. In addition, for all approaches, we require only a single image as input.

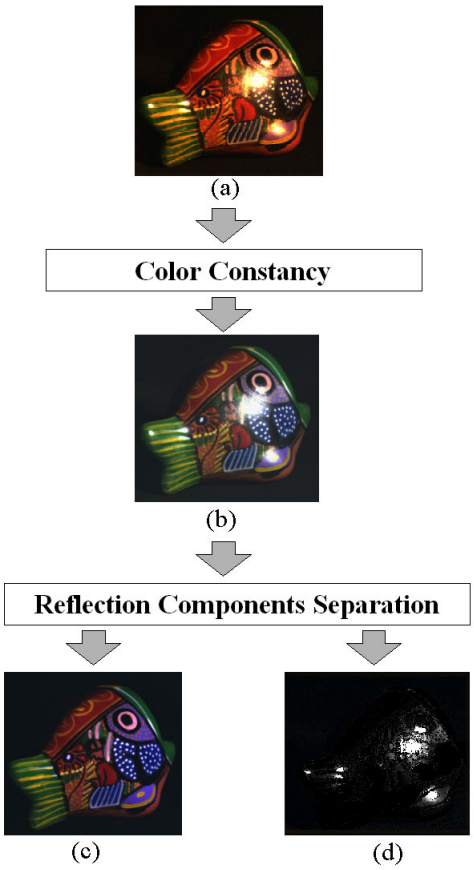

Figure 2: The flow of our framework to extract actual body color of an object. (a) Input image lit with unknown illumination. (b) Color constancy result, transforming unknown illumination color into pure-white illumination. (c) Diffuse only reflection, which is able to produce a consistent color descriptor of the object. (d) Specular only reflection, conceiving important properties such as surface roughness.

1.1 Previous Work

Color Constancy Finlayson *et al.* [11] categorized color constancy methods into two classes: statistics-based and physics-based methods. Statistics-based methods utilize the relationship between color distributions and statistical knowledge of common lights and surfaces [4, 7, 9, 34, 43, 45]. One drawback of these methods is that they require many colors to be observed on the target surfaces. On the other hand, physics-based methods [6, 8, 14, 23, 24], which base their algorithms on understanding the physical process of reflected light, can successfully deal with fewer surface colors, even to the extreme of a single surface color [11, 12]. In addition, based on the surface type of the input image, physics-based methods can be divided into two groups: diffuse-based and dichromatic-based methods. Diffuse-based methods assume that input images have only diffuse reflection, while dichromatic-based methods assume both diffuse and specular reflections occur in the images. Geusebroek *et al.* [17, 16] proposed a physical basis of color constancy by considering the spectral and spatial derivatives of the Lambertian image formation model. Andersen *et al.* [1] provided an analysis on image chromaticity under two illumination colors for dichromatic surfaces. Since our aim is to develop an algorithm that is able to handle both a single and multiple surface colors, in this section, we will concentrate our discussion on existing physics-based methods, particularly dichromatic-based methods.

Methods in dichromatic-based color constancy rely on the dichromatic reflection model proposed by Shafer [36]. Klinker *et al.* [21] introduced a method to estimate illumination color from a uniformly colored surface, by extracting a T-shaped color distribution in the RGB space. However, in real images, it becomes quite difficult to extract the T-shape due to noise, making the final estimate unreliable.

Lee [23] introduced a method to estimate illumination chromaticity using highlights of at least two surface colors. The estimation is accomplished by finding an intersection of two or more dichromatic lines in the chromaticity space. While this simple approach based on the physics of reflected light provides a handy method for color constancy, it suffers from a few

drawbacks. First, to create the dichromatic line for each surface color from highlights, one needs to segment the surface colors underneath the highlights. This color segmentation is difficult when the target object is highly textured. Second, nearly parallel dichromatic lines caused by similar surface colors can make the intersection sensitive to noise. Consequently, for real images, which usually suffered from noise, the estimation for similar surface colors becomes unstable. Third, the method does not deal with uniformly colored surfaces. Parallel to this, several methods have been proposed in the literature [6, 42, 44].

Recently, three methods have been proposed which extend Lee's algorithm [23]: Lehmann *et al.* [28] developed a more robust technique to identify the dichromatic lines in the chromaticity space. The success of this technique depends on an assumption that, in each highlight region, the surface color is uniform. As a consequence, the technique fails when dealing with complex textured surfaces, which usually have more than one surface color in their highlight regions. Finlayson *et al.* [10], proposed imposing a constraint on the colors of illumination. This constraint is based on the statistics of natural illumination colors, and improves the stability in obtaining the intersection, i.e., it addresses the second drawback of Lee's method. Furthermore, Finlayson *et al.* [11] proposed the use of the Planckian locus as a constraint to accomplish illumination estimation from uniformly colored surfaces. This Planckian constraint on the illumination chromaticity makes the estimation more robust, especially for natural scene images. However, the method still has a few drawbacks. First, the position and the shape of the Planckian locus in the chromaticity space make the estimation error prone for certain surface colors, such as blue or yellow color. Second, as they include diffuse regions in obtaining dichromatic lines, the result could become inaccurate. While the fact that their method does not require reflection separation is one of the advantages, the diffuse cluster, due to noise, usually has a different direction from the specular cluster; as a result, the dichromatic line can be shifted from the correct one. Third, like other previous methods, for multicolored surfaces, color segmentation is required.

Reflection Components Separation Many works also have been developed for separating reflection components. Wolff *et al.* [47] used a polarizing filter to separate reflection components from gray images. The main idea of their method is that, for most incident angles, diffuse reflections tend to be less polarized than the specular reflections. Nayar *et al.* [31] extended this work by considering colors instead of using the polarizing filters alone. They identified specular pixels and the illumination color vector in RGB space by using intensity variation produced by a polarizing filter. A specular pixel, which is partially composed of a specular reflection component, will have a different intensity if the polarization angle of the filter is changed. The combination of polarizing filter and colors is even for textured surfaces; however, utilizing such an additional filter is impractical in some circumstances. Sato *et al.* [35] introduced a four-dimensional space, temporal-color space, to analyze the diffuse and specular reflections based on colors and image intensity. While this method has the ability to separate the reflection components locally, since each location contains information of diffuse and specular reflections, it requires dense input images with variation of illuminant directions. Lee *et al.* [26, 27] introduced color histogram differencing to identify specularities. The key idea is that colors of diffuse pixels are independent of the changing of viewing positions, while colors of specular pixels are dependent on it. They transform the pixels of images taken from different viewing directions into RGB space, and then identify the specular pixels. Later, Lin *et al.* [29] extended this method by adding multibaseline stereo. Criminisi et al. [5] developed an Epipolar Plane Image (EPI)- based method to detect specularities. They found that in two-dimensional spatio-temporal space, highlights' straight lines have larger gradients than diffusers' straight lines. Lin *et al.* [30], unlike previous methods, introduced a method using sparse images (at least two images) under different illumination positions. They proposed an analytical method that combines the finite dimensional basis functions [33] and a dichromatic model to form a closed form equation, by assuming that the sensor sensitivity is narrowband. This method can separate the reflection component locally.

The aforementioned methods are considerably effective in separating reflection components; however, for many applications, using multiple images is impractical. Shafer [36], who introduced the dichromatic reflection model, was one of the early researchers who used a single colored image. He proposed a separation method based on parallelogram distribution of colors in RGB space. Klinker *et al.* [21] then extended this method by introducing a T-shaped color distribution. This color distribution represents body and illumination color vectors. By separating these vectors, the reflection equation becomes a closed form equation and directly solvable. Unfortunately, for many real images, this T shape is hardly extractable due to noise, etc. Bajscy *et al.* [2] proposed an approach that introduced a three dimensional space composed of lightness, saturation and hue. In their method, the input image has to be neutralized to pure-white illumination using a linear basis functions operation. For every neutralized pixel, the weighting factors of the surface reflectance basis functions are projected into the three-dimensional space, where specular and diffuse reflections are identifiable due to the difference of their saturation values.

1.2 Overview

The rest of this paper is organized as follows: in Section 2, we discuss the reflection model used in all methods proposed in this paper. In Section 3, we will explain the derivation and detail algorithm of the proposed color constancy method. In Section 4, we will focus the discussion on the method of separating reflection components. A number of experimental results using real images will be shown in Section 5. Finally, in Section 6, we offer several conclusions.

2 Reflection Model

Image Formation. Most inhomogeneous objects, such as those made of plastics, acrylics, etc., exhibit both diffuse and specular reflections. The diffuse reflection is due to the varying refractive indices in the objects' surfaces and bodies, while the specular reflection is mainly due to the refractive index difference between objects' surfaces and the air. Considering these two reflection components, Shafer [36] introduced the dichromatic reflection model, which states that reflected lights of inhomogeneous objects are linear combinations of diffuse and specular reflection components. As a result, an image's pixel of inhomogeneous objects taken by a digital color camera can be described as:

$$\mathbf{I}(\mathbf{x}) = w_d(\mathbf{x}) \int_\Omega S(\lambda, \mathbf{x}) E(\lambda) \mathbf{q}(\lambda) d\lambda + w_s(\mathbf{x}) \int_\Omega E(\lambda) \mathbf{q}(\lambda) d\lambda \quad (1)$$

where $\mathbf{I} = \{I_r, I_g, I_b\}$ is the color vector of image intensity or camera sensor. The spatial parameter, $\mathbf{x} = \{x, y\}$, is the two dimensional image coordinates. $\mathbf{q} = \{q_r, q_g, q_b\}$ is the three-element-vector of sensor sensitivity. $w_d(\mathbf{x})$ and $w_s(\mathbf{x})$ are the weighting factors for diffuse and specular reflection, respectively; their values depend on the geometric structure at location $\mathbf{x}$. $S(\mathbf{x}, \lambda)$ is the diffuse spectral reflectance function, while $E(\lambda)$ is the spectral power distribution function of illumination. $E(\lambda)$ is independent of the spatial location ($\mathbf{x}$) because we assume a uniform illumination color. The integration is done over the visible spectrum (Ω). Note that we ignore the camera

gain and camera noise in the above model, and assume that the model follows the neutral interface reflection (NIR) assumption [25], i.e., the color of specular reflection component equals the color of the illumination. For the sake of simplicity, Equation (2) can be written as:

$$\mathbf{I}(\mathbf{x}) = w_d(\mathbf{x})\mathbf{B} + w_s(\mathbf{x})\mathbf{G} \tag{2}$$

where $\mathbf{B} = \int_\Omega S(\lambda, \mathbf{x})E(\lambda)\mathbf{q}(\lambda)d\lambda$, and $\mathbf{G} = \int_\Omega E(\lambda)\mathbf{q}(\lambda)d\lambda$. The first part of the right side of the equation represents the diffuse reflection component, while the second part represents the specular reflection component.

Chromaticity Besides the dichromatic reflection model, we also use chromaticity or *normalized rgb*, which is defined as:

$$\boldsymbol{\sigma}(\mathbf{x}) = \frac{\mathbf{I}(\mathbf{x})}{I_r(\mathbf{x}) + I_g(\mathbf{x}) + I_b(\mathbf{x})} \tag{3}$$

where $\boldsymbol{\sigma} = \{\sigma_r, \sigma_g, \sigma_b\}$. Based on the equation, for the diffuse only reflection component ($w_s = 0$), the chromaticity will be independent from the diffuse weighting factor w_d. We call this *diffuse chromaticity* ($\boldsymbol{\Lambda}$) with definition:

$$\boldsymbol{\Lambda}(\mathbf{x}) = \frac{\mathbf{B}(\mathbf{x})}{B_r(\mathbf{x}) + B_g(\mathbf{x}) + B_b(\mathbf{x})} \tag{4}$$

where $\boldsymbol{\Lambda} = \{\Lambda_r, \Lambda_g, \Lambda_b\}$. On the other hand, for the specular only reflection component ($w_d = 0$), the chromaticity will be independent from the specular weighting factor (w_s), and we call it *specular* or *illumination chromaticity* ($\boldsymbol{\Gamma}$):

$$\boldsymbol{\Gamma} = \frac{\mathbf{G}}{G_r + G_g + G_b} \tag{5}$$

where $\boldsymbol{\Gamma} = \{\Gamma_r, \Gamma_g, \Gamma_b\}$. Consequently, with regard to Equation (4) and (5), Equation (2) becomes able to be written in term of chromaticity:

$$\mathbf{I}(\mathbf{x}) = m_d(\mathbf{x})\boldsymbol{\Lambda}(\mathbf{x}) + m_s(\mathbf{x})\boldsymbol{\Gamma} \tag{6}$$

where

$$m_d(\mathbf{x}) = w_d(\mathbf{x})\big[B_r(\mathbf{x}) + B_g(\mathbf{x}) + B_b(\mathbf{x})\big] \tag{7}$$

$$m_s(\mathbf{x}) = w_s(\mathbf{x})(G_r + G_g + G_b) \tag{8}$$

As a result, we have three types of chromaticity: image chromaticity ($\boldsymbol{\sigma}$), diffuse chromaticity ($\boldsymbol{\Lambda}$) and illumination chromaticity ($\boldsymbol{\Gamma}$). The image chromaticity is directly obtained from the input image using Equation (3). In addition, without loss of generality, we can have $(\sigma_r + \sigma_g + \sigma_b) = (\Lambda_r + \Lambda_g + \Lambda_b) = (\Gamma_r + \Gamma_g + \Gamma_b) = 1$.

Based on the dichromatic reflection model and chromaticities definitions derived above, we describe our goal: given image intensities ($\mathbf{I}(\mathbf{x})$) whose illumination chromaticity ($\boldsymbol{\Gamma}$) is estimated by a color constancy method; we intend to decompose them into their reflection components: $m_d(\mathbf{x})\boldsymbol{\Lambda}(\mathbf{x})$ and $m_s(\mathbf{x})\boldsymbol{\Gamma}$.

3 Color Constancy *

3.1 Inverse-Intensity Chromaticity Space

By substituting each color channel's image intensity in Equation (3) with its definition in Equation (6) and considering pixel-based operation, the image chromaticity can be written in terms of dichromatic reflection model:

$$\boldsymbol{\sigma} = \frac{m_d\boldsymbol{\Lambda} + m_s\boldsymbol{\Gamma}}{m_d[\Lambda_r + \Lambda_g + \Lambda_b] + m_s[\Gamma_r + \Gamma_g + \Gamma_b]} \tag{9}$$

*This section has similar contents to our other papers appeared in [38, 40]

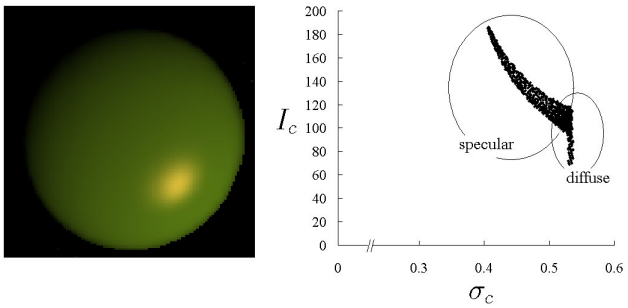

(a) (b)

Figure 3: (a) Synthetic image with a single surface color. (b) Projection of the diffuse and specular pixels into the chromaticity-intensity space, with index c representing g (the green channel).

Since $(\Lambda_r + \Lambda_g + \Lambda_b) = (\Gamma_r + \Gamma_g + \Gamma_b) = 1$, we can obtain the correlation between m_s and m_d:

$$m_s = m_d\frac{(\boldsymbol{\Lambda} - \boldsymbol{\sigma})}{(\boldsymbol{\sigma} - \boldsymbol{\Gamma})} \tag{10}$$

Then, by plugging Equation (10) into Equation (6), the correlation between image intensity ($\mathbf{I}$) and image chromaticity ($\boldsymbol{\sigma}$) can be described as:

$$\mathbf{I} = m_d(\boldsymbol{\Lambda} - \boldsymbol{\Gamma})\left(\frac{\boldsymbol{\sigma}}{\boldsymbol{\sigma} - \boldsymbol{\Gamma}}\right) \tag{11}$$

The last equation shows that the correlation between image intensity ($\mathbf{I}$) and image chromaticity ($\boldsymbol{\sigma}$) is not linear. Consequently, by projecting a uniformly colored surface into chromaticity-intensity space, the specular pixels will form a curved cluster (non-linear correlation), as illustrated in Figure 3.b. On the other hand, the diffuse pixels will form a straight vertical line, since their image chromaticity ($\boldsymbol{\sigma}$) which equals to their diffuse chromaticity ($\boldsymbol{\Lambda}$) is independent from image intensity ($\mathbf{I}$).

3.2 Image Chromaticity and Illumination Chromaticity

By introducing $\mathbf{p} = \{p_r, p_g, p_b\}$ which we define as $\mathbf{p} = m_d(\boldsymbol{\Lambda} - \boldsymbol{\Gamma})$, we can derive from Equation (11) that:

$$\frac{\mathbf{I}}{\boldsymbol{\sigma}} = \frac{\mathbf{p}}{\boldsymbol{\sigma} - \boldsymbol{\Gamma}} \tag{12}$$

Since $\mathbf{I}/\boldsymbol{\sigma} = \Sigma I_i$, where $\Sigma I_i = (I_r + I_g + I_b)$, then the correlation between image chromaticity and illumination chromaticity becomes:

$$\boldsymbol{\sigma} = \mathbf{p}\frac{1}{\Sigma I_i} + \boldsymbol{\Gamma} \tag{13}$$

This equation is the core of our method. It shows that by solely calculating the value of $\mathbf{p}$, we are able to determine the illumination chromaticity ($\boldsymbol{\Gamma}$), since image chromaticity ($\boldsymbol{\sigma}$) and total image intensity (ΣI_i) can be directly observed from the input image. Moreover, based on the equation we can solve the illumination estimation independently for each color channel, which is expressed as:

$$\sigma_c = p_c\frac{1}{\Sigma I_i} + \Gamma_c \tag{14}$$

where index c represents one of the three color channels ($\{r, g, b\}$) we want to estimate. The details are as follows.

If the values of p_c are constant and the values of ΣI_i vary throughout the image, the last equation becomes a linear equation, and the illumination chromaticity (Γ_c) can be estimated in a straightforward manner by using general line fitting algorithms for each color channel. However, in most images, the values of p_c are not constant, since p_c depends on m_d, Λ_c and Γ_c. For the sake of simplicity, until the end of this section, we temporarily assume that the values of Λ_c are constant, making the values of p_c depend solely on m_d, as Γ_c has already been assumed to be constant.

Equation (7) states that $m_d = w_d(B_r + B_g + B_b)$. According to the Lambert's Law [22], w_d is determined by the angle between lighting direction and surface normal, while $(B_r + B_g + B_b)$ is determined by diffuse albedo and intensity of incident light (L). For a surface with a uniform color, the value of the diffuse albedo is constant. The angles between surface normals and light directions depend on the shape of the object and the light distribution. The angle will be constant if an object has planar surface and illumination directions are the same for all points in the surface. While, if the surface is not planar or the illumination directions are not uniform, then the angle will vary. The values of intensity of incident light (L) are mostly determined by the location of illuminants, which will be constant if the locations of the illuminants are distant from the surface. For relatively nearby illuminants, the values of L may vary w.r.t. the surface point. Considering all these aspects, as a result, in general conditions the value of m_d can be either constant or varied. Yet, in most cases the value of m_d will be varied because, most shapes of objects in the real world are not planar and the assumption on uniform illumination direction, in some conditions, cannot be held.

Consequently, Equation (14) poses two problems: first, whether there are a number of specular pixels that have the same m_d, and second, whether these pixels that have the same m_d also have different ΣI_i. If we consider a single surface color, then the solution of the first problem depends on w_d and L. In microscopic scale of the real world, the combination of w_d and L could be unique. Fortunately, in the scale of image intensity, for some set of surface points, the differences of the combination of w_d and L are small and can be approximated as constant. We can take this approximation for granted, as current ordinary digital cameras automatically do it for us as a part of their accuracy limitation.

The second problem can be resolved by considering Equation (6). In this equation, two specular pixels will have the same m_d but different $\mathbf{I}$, if their values of m_s are different. Equation (8) states that $m_s = \tilde{w}_s(G_r + G_g + G_b)$. In Torrance and Sparrow reflection model [46], which is reasonably accurate to model specularity, $\tilde{w}_s$ is expressed as:

$$\tilde{w}_s = FG\frac{1}{cos\theta_r}exp(-\frac{\alpha^2}{2\phi^2}) \qquad (15)$$

where F is the Fresnel reflection, G is the geometrical attenuation factor, θ_r is the angle of surface normal and viewing direction, α is the angle between the surface normal and the bisector of viewing direction and illumination direction, and ϕ is the surface roughness. Thus, if the two specular pixels have the same surface color lit by distant light source and have the same m_d which implies the same $\mathbf{p}$, then m_s of both pixels will be different if their values of θ_r and α are different.

Hence, in general conditions, specular pixels can be grouped into a number of clusters that have the same values of p_c and different ΣI_i. For every group of pixels that share the same or approximately the same value of m_d, we can consider p_c as a constant, which makes Equation (14) become a linear equation, with p_c as its constant gradient. These groups of pixels can be clearly observed in inverse-intensity chromaticity space, with x-axis representing $1/\Sigma I_i$ and y-axis representing σ_c, as illustrated in Figure 4.a. Several straight lines in the figure correspond to several groups of different m_d values (several number of different p_c: $p_c^1,\ldots, p_c^j,\ldots, p_c^n$, where c is identical to the

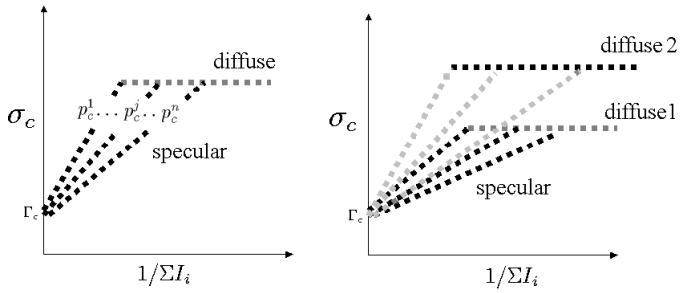

Figure 4: (a) Sketch of specular points of uniformly colored surface in inverse-intensity chromaticity space. (b) Sketch of specular points of two surface different colors.

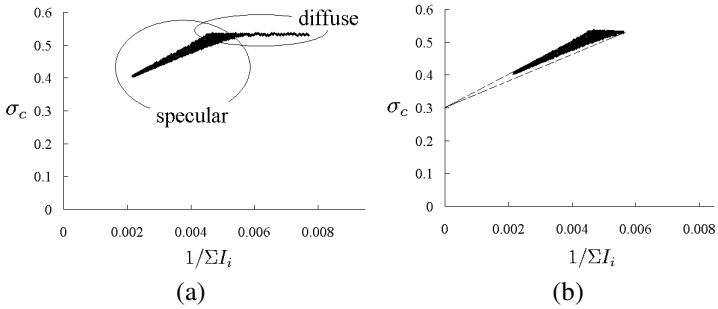

Figure 5: (a) Diffuse and specular points of a synthetic image (Figure 3.a) in inverse-intensity chromaticity space, with c representing the green channel. (b) The cluster of specular points which head for illumination chromaticity value in y-axis

c of σ_c). These lines intersect at a single point on the y-axis, which is identical to the illumination chromaticity (Γ_c). Figure 5.a shows the projection of all pixels of a synthetic image in Figure 3.a into inverse-intensity chromaticity space. The horizontal line in the figure represents the diffuse points, since the image chromaticity of diffuse pixels will be constant regardless the change of ΣI_i. While, the slant cluster represents the specular points. If we focus on this cluster by removing the diffuse points, according to Equation (14) we will find that a number of straight lines, which compose the cluster, head for the value of illumination chromaticity at y-axis, as shown in Figure 5.b.

Now we relax the assumption of uniformly colored surface to handle multicolored surfaces. Figure 4.b. illustrates the projection of two different surface colors into inverse-intensity chromaticity space. We can observe two specular clusters with different values of diffuse chromaticity head for the same value on the chromaticity axis (Γ_c). Since we only consider points that have the same values of p_c and Γ_c, then even if there are

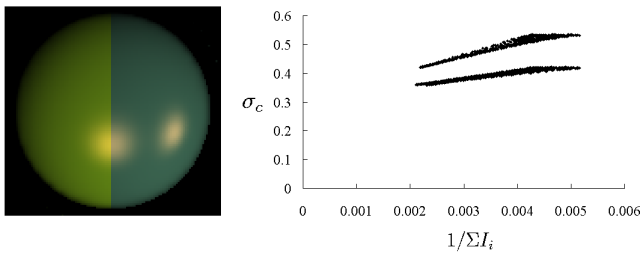

Figure 6: (a) Synthetic image with multiple surface colors. (b) Specular points in inverse-intensity chromaticity space, with c representing the green channel.

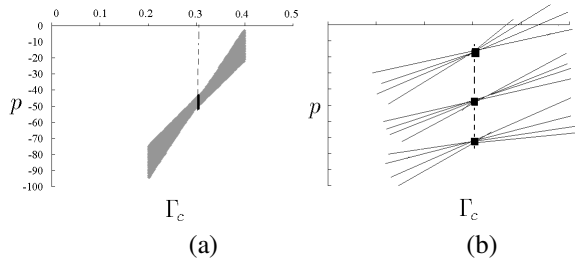

Figure 7: (a) Projection of points in Figure 5.b into Hough space. (b) Sketch of intersected lines in Hough space.

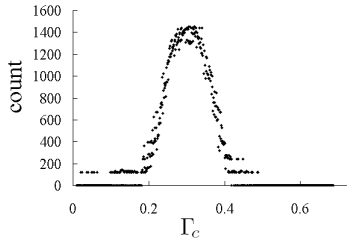

Figure 8: Intersection-counting distribution of the green channel. The estimated illumination chromaticity is as follows: $\Gamma_r = 0.535$, $\Gamma_b = 0.303$, $\Gamma_b = 0.162$, the ground-truth values are: $\Gamma_r = 0.536, \Gamma_b = 0.304, \Gamma_b = 0.160$.

many different clusters with different values of Λ_c, as is the case for multicolored surfaces, we can still safely estimate the illumination chromaticity (Γ_c). This means that, for multicolored surfaces, the estimation process is exactly the same to the case of a uniformly colored surface. Figure 6.b shows the projection of hightlighted regions of a synthetic image with two surface colors (Figure 6.a) into inverse-intensity chromaticity space.

3.3 Computational Method

To estimate every value of illumination chromaticity ($\{\Gamma_r, \Gamma_g, \Gamma_b\}$) from inverse-intensity chromaticity space, we use the Hough transform for each color channel. Figure 7.a shows the transformation from inverse-intensity chromaticity space into the Hough space, where its x-axis represents Γ_c with index c representing color channel we want to estimate, and its y-axis represents p_c, with c equals the c of Γ_c. Since Γ_c is a normalized value, the range of its value is from 0 to 1 ($0 < \Gamma_c < 1$).

Using the Hough transform alone does not yet give any solution, because the values of p_c are not constant throughout the image, which makes the intersection point of lines not located at a single location. Fortunately, even if the values of p_c vary, the values of Γ_c are constant. Thus, in principle, all intersections will be concentrated at a single value of Γ_c, with a small range of p_c's values. These intersections are indicated by a thick solid line in Figure 7.a. If we focus on the intersections in the Hough space as illustrated in Figure 7.b, we should find a larger number of intersection at a certain value of Γ_c compared to other values of Γ_c. The reason is, in inverse-intensity chromaticity space, within the range of Γ_c ($0 < \Gamma_c < 1$), the number of groups of points that form a straight line heading for certain value of Γ_c are more dominant than the number of groups of points that form a straight line heading for other values of Γ_c.

In practice, we count the intersections in the Hough space based on the number of points that occupy the same location. The details are as follows. A line in the Hough space is formed by a number of points. If this line is not intersected by other lines, then each point will occupy a certain location uniquely (one point for each location). However, if two lines intersect, a location where the intersection takes place will be shared by two points. The number of points will increase if other lines also intersect with those two lines at the same location. Thus, to count the intersections, we first discard all points that occupy a location uniquely, as it means there are no intersections, and then count the number of points for each value of Γ_c.

As a consequence, by projecting the total number of intersections of each Γ_c into a two-dimensional space, illumination-chromaticity count space, with y-axis representing the count of intersections and x-axis representing Γ_c, we can robustly estimate the actual value of Γ_c. Figure 8.a shows the distribution of the count numbers of intersections in the space, where the distribution forms a Gaussian-like distribution. The peak of the distribution lies at the actual value of Γ_c.

3.4 Implementation

Implementation of the proposed method is quite simple. Given an image that has highlights, we first find the highlight regions by using thresholding on image intensity and saturation values. Following the method of Lehmann *et al.* [28], we define the threshloding as follows:

$$\begin{aligned} \tilde{I} &= \frac{I_r + I_g + I_b}{3} > T_a \tilde{I}^{max} \\ \tilde{S} &= 1 - \frac{min(I_r, I_g, I_b)}{\tilde{I}} < T_b \tilde{S}^{max} \end{aligned} \quad (16)$$

where $\tilde{I}^{max}$ and $\tilde{S}^{max}$ are the largest $\tilde{I}$ and $\tilde{S}$ in the whole input image, respectively. T_a and T_b are the thresholds of image intensity and saturation, respectively. In our implementation, we set T_a and T_b from $0.4 - 0.6$.

This thresholding technique cannot always produce precise highlight regions. Fortunately, in practice our estimation method does not need precise highlight region, even if relatively small regions of diffuse pixels are included, the algorithm could work robustly. Of course, more preciseness is better. Then, for each color channel, we project the highlight pixels into inverse-intensity chromaticity space. From this space, we use the conventional Hough transform to project the clusters into Hough space. During the projection, we count all possible intersections at each value of chromaticity. We plot these intersection-counting numbers into the illumination-chromaticity count space. Ideally, from this space, we can choose the tip as the estimated illumination chromaticity. However, as noise always exists in real images, the result can be improved by computing the median of a certain percentage from the highest counts. In our implementation, we use 30% from the highest counted number.

Note that, first, in our current implementation we estimate three color channels of illumination chromaticity independently. In fact, since $(\Gamma_r + \Gamma_g + \Gamma_b) = 1$, we can solely estimate two color channels instead of three color-channels. Second, the problem of determining highlight regions is still an open challenging problem, and our method could fail for specific domains that do not follow our thresholding described in Equation (16).

4 Reflection Components Separation †

4.1 Normalization

In our method, to separate reflection components correctly, the color of the specular component must be pure white ($\Gamma_r = \Gamma_g = \Gamma_b$). So, we need to normalize the input image. The normalization requires the value of $\mathbf{\Gamma}$ (illumination chromaticity), which can be estimated using color constancy algorithms explained in Section 3, or using white reference. We express

† This section has similar contents to our paper appeared in [37]

the estimated illumination chromaticity as $\mathbf{\Gamma}^{est}$, with $\mathbf{\Gamma}^{est} = \{\Gamma_r^{est}, \Gamma_g^{est}, \Gamma_b^{est}\}$, and the normalized image as:

$$\mathbf{I}'(\mathbf{x}) = m_d(\mathbf{x})\mathbf{\Lambda}'(\mathbf{x}) + m_s(\mathbf{x}) \tag{17}$$

where $\mathbf{I}'(\mathbf{x}) = \frac{\mathbf{I}(\mathbf{x})}{\mathbf{\Gamma}^{est}}$, the normalized image intensity and $\mathbf{\Lambda}' = \frac{\mathbf{\Lambda}(\mathbf{x})}{\mathbf{\Gamma}^{est}}$, the normalized diffuse chromaticity, and we assume $\frac{\mathbf{\Gamma}}{\mathbf{\Gamma}^{est}} = \{1, 1, 1\}$. Using the above normalization, we can obtain a scalar value of the specular reflection component.

Later, when the separation is done, to obtain the actual reflection components, we need to renormalize the separated components, simply by multiplying them $\Big(m_d(\mathbf{x})\mathbf{\Lambda}'(\mathbf{x})$ and $m_s(\mathbf{x})\Big)$ with $\mathbf{\Gamma}^{est}$:

$$m_d(\mathbf{x})\mathbf{\Lambda}(\mathbf{x}) = \Big[m_d(\mathbf{x})\frac{\mathbf{\Lambda}(\mathbf{x})}{\mathbf{\Gamma}^{est}}\Big]\mathbf{\Gamma}^{est} \tag{18}$$

$$m_s(\mathbf{x})\mathbf{\Gamma} = \Big[m_s(\mathbf{x})\frac{\mathbf{\Gamma}}{\mathbf{\Gamma}^{est}}\Big]\mathbf{\Gamma}^{est} \tag{19}$$

4.2 Specular-free Image

To deal with multicolored surfaces we utilize *specular-to-diffuse mechanism* [37, 39, 41]. By utilizing the mechanism, the problem of separation can be simplified into the problem of finding diffuse maximum chromaticity; and, principally for uniformly colored surface, we can find it from the largest value of maximum chromaticity (the extreme right point in maximum chromaticity intensity space). Unfortunately, unlike uniformly colored surfaces, the diffuse maximum chromaticities for multicolored surfaces are completely unknown, which in fact, is the main problem of separating reflection component using a single multicolored image. Thus, for multicolored surfaces, the specular-to-diffuse mechanism cannot be applied directly.

Nevertheless, the mechanism is still useful, since it informs us that the diffuse component of a specular point lies somewhere in the curved line. A brief about the mechanism is as follows. First, we define maximum chromaticity as:

$$\tilde{\sigma'}(\mathbf{x}) = \frac{\tilde{I'}(\mathbf{x})}{I'_r(\mathbf{x}) + I_g\prime(\mathbf{x}) + I_b\prime(\mathbf{x})} \tag{20}$$

where $\tilde{I'}(\mathbf{x}) = max(I'_r(\mathbf{x}), I'_g(\mathbf{x}), I'_b(\mathbf{x}))$. Unlike normalized image chromaticity ($\boldsymbol{\sigma}$), $\tilde{\sigma}'$ is a scalar value. Using the maximum chromaticity definition, we describe the correlation of image intensity, $\tilde{I}'$, and image chromaticity, $\tilde{\sigma}'$, as (see Appendix A for detail derivation):

$$\tilde{I'}(\mathbf{x}) = m_d(\mathbf{x})(\tilde{\Lambda}'(\mathbf{x}) - 1/3)\Big(\frac{\tilde{\sigma}'(\mathbf{x})}{\tilde{\sigma}'(\mathbf{x}) - 1/3}\Big) \tag{21}$$

where $\tilde{\Lambda}'$ has identical color channel to $\tilde{I}$. Then, the specular-to-diffuse mechanism mathematically can be expressed as:

$$m_d(\mathbf{x}) = \frac{\tilde{I'}(\mathbf{x})[3\tilde{\sigma}'(\mathbf{x}) - 1]}{\tilde{\sigma}'(\mathbf{x})[3\tilde{\Lambda}'(\mathbf{x}) - 1]} \tag{22}$$

$$m_s(\mathbf{x}) = \frac{1}{3}[(I'_r(\mathbf{x}) + I'_b(\mathbf{x}) + I'_g(\mathbf{x})) - m_d(\mathbf{x})] \tag{23}$$

$$m_d(\mathbf{x})\mathbf{\Lambda}'(\mathbf{x}) = \mathbf{I}'(\mathbf{x}) - m_s(\mathbf{x}) \tag{24}$$

One significant appliance of specular-to-diffuse mechanism is to generate a *specular-free image*, an image that is free from highlights and has geometrical profile identical to the diffuse component of the input image. To generate it, we simply set the

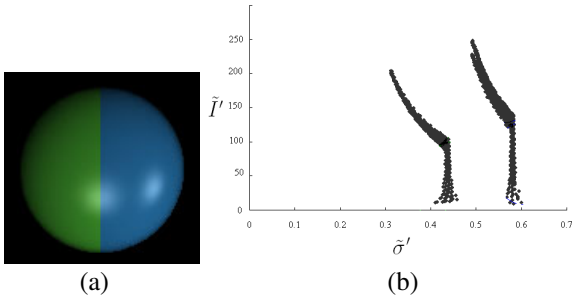

(a) (b)

Figure 9: (a) Synthetic image. (b) Projection of the synthetic image pixels into the maximum chromaticity intensity space.

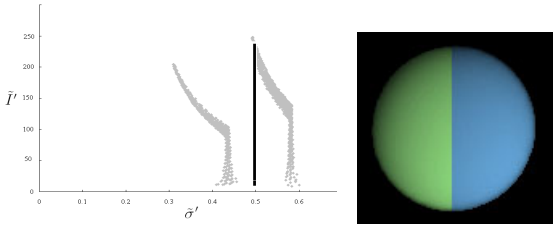

(a) (b)

Figure 10: (a) Shifting all pixels into arbitrary $\tilde{\Lambda}'$. (b) Specular-free image.

diffuse maximum chromaticity ($\tilde{\Lambda}'$ in Equation (22)) equal to an arbitrary scalar value ($1/3 < \tilde{\Lambda}' \leq 1$), for all pixels regardless of their color. For instance, we set $\tilde{\Lambda}'$ equal to 0.5 for image in Figure 9.a, which implies that the distribution of the points in maximum chromaticity-intensity space becomes a vertical line as shown in Figure 10.a. As a result, we can obtain an image that does not have specular reflections (Figure 10.b). Figure 11.a shows a real image of a multicolored scene. By setting $\tilde{\Lambda}' = 0.5$ for all pixels, we obtain an image that is geometrically identical to the diffuse component of the input image (Figure 11.b). The difference of both is solely in their surface colors.

This technique can successfully remove highlights mainly because the saturation values of all pixels are made constant (with regard to the maximum chromaticity) while retaining their hue [6, 2]. It is well known that, if the specular component's color is pure white, then diffuse and specular pixels that have the same surface color will have identical values of hue, with the hue defined as [18]:

$$H = cos^{-1}\left[\frac{\frac{1}{2}\Big[(I'_r - I'_g) + (I'_r - I'_b)\Big]}{\Big[(I'_r - I'_g)^2 + (I'_r - I'_b)(I'_g - I'_b)\Big]^{\frac{1}{2}}}\right] \tag{25}$$

but difference saturation values, with saturation is defined as [18]:

$$S = 1 - \Big[\frac{3}{I'_r + I'_g + I'_b} min(I'_r, I'_g, I'_b)\Big] \tag{26}$$

In our dichromatic reflection model (Equation 17), different saturation means different value of m_s (the weighting factor of specular component), and the same hue means the same value of $\mathbf{\Lambda}'$ (the normalized diffuse chromaticity). As consequences, in maximum chromaticity intensity space, for diffuse points with the same $\mathbf{\Lambda}'$, both saturation and hue values will be constant (since their m_s values equal zero). In contrast, for specular points, the saturation values will vary (since their m_s values vary), and if their diffuse chromaticities are the same, the hue values will be constant. Thus, shifting all points in maximum

(a) (b)

Figure 11: (a) Normalized image after removing achromatic pixels, below-camera-dark pixels and saturated pixels (b) Specular-free image by setting $\tilde{\Lambda} = 0.5$. The specular components are perfectly removed; the difference is only in the surface color.

chromaticity intensity space into a certain arbitrary value using a specular-to-diffuse mechanism is identical to making all points' saturation values constant while retaining their hue values intact. These constant-saturation values cause the highlights to disappear from the image.

Formally, we can describe the specular-free image as:

$$\mathring{\mathbf{I}}(\mathbf{x}) = \mathring{m}_d(\mathbf{x})\mathring{\mathbf{\Lambda}}(\mathbf{x}) \tag{27}$$

where $\mathring{\mathbf{I}}(\mathbf{x}) = \{\mathring{I}_r(\mathbf{x}), \mathring{I}_g(\mathbf{x}), \mathring{I}_b(\mathbf{x})\}$ is the image intensity of the specular-free image, $\mathring{\mathbf{\Lambda}}(\mathbf{x}) = \{\mathring{\Lambda}_r(\mathbf{x}), \mathring{\Lambda}_g(\mathbf{x}), \mathring{\Lambda}_b(\mathbf{x})\}$ is the diffuse chromaticity, and $\mathring{m}_d$ is the diffuse weighting factor. In the following, we will prove that $\mathring{m}_d$ has the same geometrical profile to m_d (the diffuse weighting factor of normalized image).

According to Equation (17) a normalized diffuse pixel is described as $\mathbf{I}'(\mathbf{x}) = m_d(\mathbf{x})\mathbf{\Lambda}'(\mathbf{x})$. If we apply the specular-to-diffuse mechanism to the pixel by substituting the value of $\tilde{\Lambda}'$ in Equation (22) where $\tilde{\Lambda}' = max(\Lambda'_r, \Lambda'_g, \Lambda'_b)$ with an arbitrary maximum chromaticity whose value equals $max(\mathring{\Lambda}_r, \mathring{\Lambda}_g, \mathring{\Lambda}_b)$, then the equation becomes:

$$\mathring{m}_d(\mathbf{x}) = \frac{\tilde{I}'(\mathbf{x})[3\tilde{\sigma}'(\mathbf{x}) - 1]}{\tilde{\sigma}'(\mathbf{x})[3max(\mathring{\Lambda}_r, \mathring{\Lambda}_g, \mathring{\Lambda}_b) - 1]} \tag{28}$$

Since $\tilde{I}'(\mathbf{x}) = m_d(\mathbf{x})\tilde{\Lambda}'(\mathbf{x})$, and for diffuse pixels $\tilde{\Lambda}'(\mathbf{x}) = \tilde{\sigma}'(\mathbf{x})$, by defining $\tilde{\Lambda}^{new} = max(\mathring{\Lambda}_r, \mathring{\Lambda}_g, \mathring{\Lambda}_b)$, we can obtain:

$$\mathring{m}_d(\mathbf{x}) = m_d(\mathbf{x})\frac{3\tilde{\Lambda}'(\mathbf{x}) - 1}{3\tilde{\Lambda}^{new} - 1} \tag{29}$$

$\tilde{\Lambda}^{new}$ is independent of the spatial parameter $(\mathbf{x})$, since we use the same value $\tilde{\Lambda}^{new}$ for all pixels regardless of their colors. Note that the same value of $\tilde{\Lambda}^{new}$ does not necessarily imply the same value $\mathring{\mathbf{\Lambda}}$. As a result, for diffuse pixels with the same diffuse chromaticity (the same surface color), $\frac{3\tilde{\Lambda}'(\mathbf{x})-1}{3\tilde{\Lambda}^{new}-1}$ will be constant, thereby enabling us to describe the image intensity of specular-free image as:

$$\mathring{\mathbf{I}}(\mathbf{x}) = m_d(\mathbf{x})k\mathring{\mathbf{\Lambda}}(\mathbf{x}) \tag{30}$$

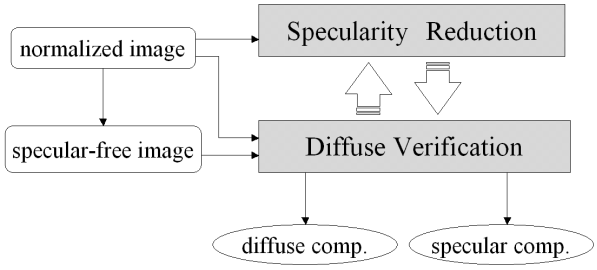

Figure 12: Basic Flow of the proposed method.

where $k = \frac{3\tilde{\Lambda}'(\mathbf{x})-1}{3\tilde{\Lambda}^{new}-1}$, a constant scalar value for pixels with the same diffuse chromaticity (pixels that are not located at color discontinuities). The proof for specular pixels is described in Appendix B. Therefore, since $\mathring{m}_d(\mathbf{x}) = m_d(\mathbf{x})k$, the diffuse geometrical profile of the specular-free image is identical to the geometrical profile of both the normalized image (17) and the input image (6).

Note that, in order to avoid generating negative values of $\mathring{\mathbf{I}}(\mathbf{x})$, the arbitrary scalar value of maximum diffuse chromaticity ($\tilde{\Lambda}^{new}$) should be chosen from a value near the smallest maximum chromaticity of the input image. Also, caution should be taken in using a specular-free image, particularly for applications that require evaluating color discontinuities since, in the case of two adjacent colors that have the same hue but different saturation, color discontinuities of the two colors will disappear.

Generating a specular-free image using specular-to-diffuse mechanism is a one-pixel-based operation that requires only a single colored image without any segmentation process. As a result, it is simple and probably useful for many applications in computer vision that do not need actual surface color but suffer from highlights.

4.3 Separation Method

Figure 12 shows the basic idea of our proposed method. First, given a normalized image, we generate a specular-free image. Based on the image, in the "diffuse verification" process, we verify whether the normalized image has diffuse-only pixels. If so, the processes terminate; otherwise, in the "specularity reduction" process, we decrease the intensity of the image's specular pixels. After that, we verify once again whether the decreased image has diffuse-only pixels in the "diffuse verification" process. These two processes (diffuse verification and specularity reduction) are done iteratively until there is no specularity in the normalized image. To accomplish their tasks, the two processes require only two adjacent pixels. This local operation is indispensable in dealing with highly textured surfaces. The following subsections will show how the two processes are carried out.

4.4 Diffuse Pixels Verification

Intensity Logarithmic Differentiation Given one colored pixel, to determine whether it is diffuse or specular pixel is completely an ill posed problem. In a linear equation such as equation (17), only from a single $\mathbf{I}'$, whether m_s is equal to zero is undeterminable. In this section, instead of a single pixel, we will show that two-neighboring pixels can be the minimum requirement to determine whether both of them are diffuse pixels.

We base our technique on intensity logarithmic differentiation of the normalized image and the specular free image. Considering a diffuse pixel which is not located at color discontinuity, we can describe it as: $\mathbf{I}'(\mathbf{x_1}) = m_d(\mathbf{x_1})\mathbf{\Lambda}'$.

The spatial parameter ($\mathbf{x_1}$) is removed from $\mathbf{\Lambda}'$, since the pixel is not located at color discontinuity. If we apply logarithmic and then differentiation operation on this pixel, the equation becomes:

$$log(\mathbf{I}'(\mathbf{x_1})) = log(m_d(\mathbf{x_1})) + log(\mathbf{\Lambda}') \quad (31)$$

$$\frac{d}{d\mathbf{x}} log(\mathbf{I}'(\mathbf{x_1})) = \frac{d}{d\mathbf{x}} log(m_d(\mathbf{x_1})) \quad (32)$$

For the same pixel's location ($\mathbf{x_1}$), we can obtain a corresponding pixel in the specular-free image. This pixel has exactly the same diffuse geometrical profile as that of the input image; only its diffuse chromaticity is different. We describe it as: $\mathring{\mathbf{I}}(\mathbf{x_1}) = m_d(\mathbf{x_1}) k \mathring{\mathbf{\Lambda}}$ where k and $\mathring{\mathbf{\Lambda}}$ are independent from spatial parameter. Thus, using the same operations, logarithmic and differentiation, we can obtain:

$$\frac{d}{d\mathbf{x}} log(\mathring{\mathbf{I}}(\mathbf{x_1})) = \frac{d}{d\mathbf{x}} log(m_d(\mathbf{x_1})) \quad (33)$$

which is exactly the same result as the pixel from the normalized image (Equation (32)). As a result, based on the intensity logarithmic differentiation operation, we become able to determine whether two-neighboring pixels are diffuse pixels (in discrete operation, the differentiation requires at least two-neighboring pixels):

$$\Delta(\mathbf{x}) = dlog(\mathbf{I}'(\mathbf{x})) - dlog(\mathring{\mathbf{I}}(\mathbf{x})) \quad (34)$$

$$\Delta(\mathbf{x}) \begin{cases} = 0 & : \text{ diffuse} \\ \neq 0 & : \text{ specular or color discontinuity} \end{cases} \quad (35)$$

As shown in Equation (35), for pixels located at color discontinuities, there is still an ambiguity between specular and color discontinuity pixels. Since using two neighboring pixels that have different surface color, the difference of the logarithmic differentiation does not equal zero, although the pixels are diffuse pixels. Theoretically, by extending the number of pixels into at least four neighboring pixels, it is possible to distinguish them. However, in real images, camera noise and surface noise (surface variance) [19, 39, 41] make such identification become error-prone. Consequently, to deal with the color is continuity problem, we need another more robust analysis which will be described in the next subsection.

Color Discontinuity A number of methods have been proposed to solve the color discontinuity problem, which is also known as the problem of material changes [20, 15]. Unlike most of the existing methods, we use a simple chromaticity-based method to handle the problem. We define $\sigma'_r = \frac{I'_r}{I'_r+I'_g+I'_b}$ and $\sigma'_g = \frac{I'_g}{I'_r+I'_g+I'_b}$, and use the below decision rule:

$$(\Delta r > thR \quad \text{and} \quad \Delta g > thG) \begin{cases} true & : \text{ color discontinuity} \\ false & : \text{ otherwise} \end{cases} \quad (36)$$

where thR and thG are the small scalar numbers. $\Delta r(\mathbf{x}) = \sigma'_r(\mathbf{x}) - \sigma'_r(\mathbf{x}-\mathbf{1})$ and $\Delta g(\mathbf{x}) = \sigma'_g(\mathbf{x}) - \sigma'_g(\mathbf{x}-\mathbf{1})$. We obtain the values of σ'_r and σ'_g from the pixels of the normalized image. This simple technique is similar to the method proposed by Funt *et al.* [13].

For two neighboring pixels, this simple chromaticity thresholding is sufficient. Since when two neighboring pixels have the same surface color, their chromaticity difference is small, even for specular pixels. This is one of the advantages of our local, two-neighboring-pixels operation. Moreover, the above thresholding can also solve the problem of two adjacent objects that have the same hue but different saturation, as long as the saturation difference is not less than the thresholds. Fortunately, in practice, even if the saturation difference is less than the thresholds, it does not affect the result much; since it implies that the objects have almost the same color, so that it is unnecessary to distinguish them. In addition, we have no problem when the above thresholding wrongly deems the shadow boundary to be a color discontinuity, since we have nothing to do with shadow.

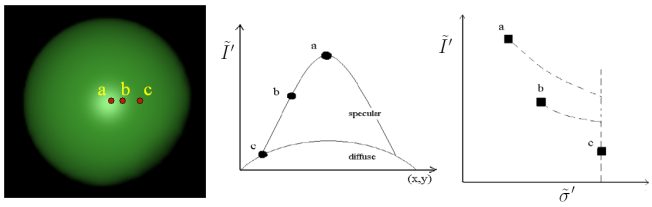

Figure 13: (a) Three points in an image. (b) The three points in spatial-intensity space. (c) The three points in maximum chromaticity intensity space.

4.5 Specularity Reduction

Specularity reduction is the second process of the two main processes we have proposed. The purpose of this process is to decrease the intensity of the specular pixels until we obtain diffuse only reflection. All operations in this process are still based only on two-neighboring pixels. Figure 13.a shows three pixels: a, b, and c. For the sake of simplicity, for the moment we assume a uniformly colored surface and that the three pixels are adjacent spatially to each other. Pixel a is the highlight's brightest pixels, and pixel c is a diffuse pixel, and pixel b is a specular pixels located between pixels a and c. In spatial-image intensity space, the image intensity of pixel a will be the largest value followed by pixels b and c, as shown in Figure 13.b. If we transform the pixels into maximum chromaticity-intensity space, we will obtain a point distribution illustrated in Figure 13.c.

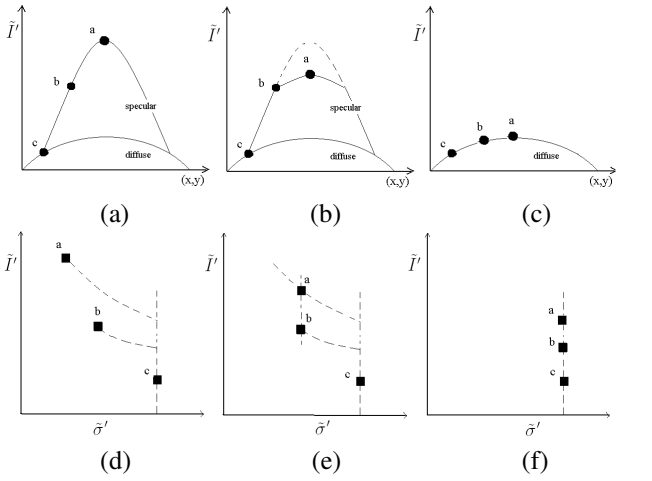

Figure 14: Basic idea of the iterative framework using local two-pixels operation. Top row, spatial-intensity space: (a) Initial condition. (b) First looping. (c) Final condition; Bottom row, chromaticity intensity space: (d) Initial condition. (e) First looping. (f) Final condition.

Figure 14 illustrates the basic idea of our specularity reduction. In considering a two-pixel operation, the iteration begins with comparing the maximum chromaticity of point a and point b in Figure 14.d . From the maximum chromaticity definition in Equation (20), we know that the smaller the m_s is, the bigger the maximum chromaticity value. In other words, point b is more diffuse than point a. Thus, by shifting point a using the

specular-to-diffuse mechanism w.r.t the maximum chromaticity of point b, the more diffuse pixel a can be obtained, i.e., the intensity of pixel a becomes decreased and its chromaticity becomes identical to point b's, as illustrated in Figure 14.b and 14.e, respectively. Using the same process in the second iteration, the maximum chromaticity of point b and point c are compared and then shifted. When the maximum chromaticity of point b equals the maximum chromaticity of point c, the intensity of pixel b becomes equal to its diffuse component. The same operation is done for all pixels iteratively until their maximum chromaticity becomes the same (Figure 14.f), which as a result, produces the diffuse components of the three pixels (Figure 14.c).

However, the above termination condition, looping until the maximum chromaticity of all pixels is the same, is feasible only for a uniformly colored surface. In multicolored surfaces, such a termination condition will produce incorrect separation results. Thus, to verify whether the image contains only diffuse pixels, we use the logarithmic differentiation, as explained in Subsections 5.4.1. Algorithm 4.1 shows the pseudo-code of the iteration method for both uniform and multicolored surfaces; a detailed explanation will be provided in Section 4.6.

4.6 Implementation

Algorithm 4.1 shows the pseudo-code of the iterative algorithm. It begins with executing function $delta(N, S, \epsilon)$, which computes the difference of the intensity logarithmic differentiation of the normalized image (N) and the specular-free image (S). In discrete operations, the logarithmic differentiation is done using: $dlog(I'_{tot}(\mathbf{x})) = log(\Sigma I'_i(\mathbf{x}+1)) - log(\Sigma I'_i(\mathbf{x}))$, where $\Sigma I'_i = (I'_r + I'_g + I'_b)$. Then, the function computes $\Delta = dlog(I'_{tot}(\mathbf{x})) - dlog(\mathring{I}_{tot}(\mathbf{x}))$, and labels the pixels of the normalized image; for pixels that have Δ more than ϵ (≈ 0), they are labeled "specular", otherwise "diffuse".

Algorithm 4.1: ITERATION(N, S, ϵ)

comment: N=normalized-image; S= specular-free-image

(1) $\Delta = delta(N, S, \epsilon)$;
(2) **while** $any(\Delta(\mathbf{x}) > \epsilon)$
  for $\mathbf{x} \leftarrow 0$ **to** sizeof(N)-1
    (3) **if** $\mathbf{x}.flag == diffuse$
      then next($\mathbf{x}$);
    (4) **if** $IsDiscontinuity(\mathbf{x}, \mathbf{x}+\mathbf{1}) == true$
      then $\mathbf{x}.flag = discontinuity$; $(\mathbf{x}+\mathbf{1}).flag = discontinuity$; $next(\mathbf{x})$;
    (5) **if** $\tilde{c}(\mathbf{x}) == \tilde{c}(\mathbf{x}+\mathbf{1})$
      then $\mathbf{x}.flag = noise$; $(\mathbf{x}+\mathbf{1}).flag = noise$; next($\mathbf{x}$);
    (6) $M(\mathbf{x}) = Specular2Diffuse(\mathbf{I}'(\mathbf{x}), \mathbf{I}'(\mathbf{x}+\mathbf{1}))$;
    next($\mathbf{x}$);
  $N = M$;
  (7) $\Delta = delta(N, S, \epsilon)$;
return (N)
comment: N = normalized diffuse component

In Step 2 until Step 4, if there are any pixels labeled "specular", for each of them, the algorithm examines whether the pixel and its neighbor are color discontinuity pixels. If so, then they are labeled "discontinuity;" otherwise, then at least one of them must be a specular pixel. In Step 5, before we apply the specular-to-diffuse mechanism to both pixels, additional checking is necessary, i.e., whether both pixels' maximum chromaticity is the same. If they are the same, then the pixels are labeled "noise". The reason that they are noise and not specular pixels is because two-neighboring specular pixels never have the same maximum chromaticity.

In Step 6, using the specular-to-diffuse mechanism the intensity and maximum chromaticity value of the pixel that have smaller $\tilde{\sigma}'$ is shifted w.r.t. the pixel with bigger $\tilde{\sigma}'$. This is applied to all pixels, and produces a more diffuse normalized image. By setting N equal to this image (M), function $delta(N, S, \epsilon)$ is executed once again in Step 7. This time, pixels labeled "discontinuity" and "noise" are ignored (not included in the process). Finally, if there is still any Δ larger than ϵ, then the iteration continues; if not, the separation terminates, which consequently, yields a diffuse component of the normalized image.

In our implementation, we define $\epsilon = 0$. For color discontinuity thresholds (thR and thG), we set them with the same number ranging from 0.05 to 0.1. The numbers are chosen by considering camera noise, illumination color variance, ambient light (some considerably small interreflections) and surface color variance (although human perception deems that the color surface is uniform, there is, in fact, still color variance due to dust, imperfect painting, etc. [39, 41]). For a more stable and robust algorithm we add an algorithm that controls the decrease of the threshold of Δ step-by-step, as described in Algorithm 4.2. In function $Iteration(N, S, \epsilon)$, $stepTh$ will replace ϵ, which in our implementation its initial value isequal to 0.5. Ideally, the initial value should be set as large as possible; yet, by considering the time computation the number is chosen. To obtain more accurate results, the smaller subtracting number (δ) is preferable and, in our implementation, we set it equal to 0.01. To anticipate regions having achromatic pixels ($I'_r = I'_g = I'_b$), which are inevitable in the real images, we remove them by using simple thresholding in maximum chromaticity; achromatic pixels of normalized image have maximum chromaticity near $1/3$. In addition, to avoid saturated pixels, HDR (High Dynamic Range) images or a diffuser filter can be used.

Algorithm 4.2: CONTROLLEDTHRESHOLD(N, S)

comment: N=normalized-image; S= specular-free-image

$RemoveAchromaticPixels(N)$;
$stepTH = InitialThreshold$;
while $stepTH > \epsilon$
  $\Delta = delta(N, S, \epsilon)$;
  if $any(\Delta(\mathbf{x}) > stepTH)$
    then $Iteration(N, S, stepTH)$;
  $stepTH = stepTH - \delta$;
  $ResetAllLabels()$;
$Renormalization(N)$;
return (N);
comment: N=actual diffuse component

5 Experimental Results

Experimental Conditions We have conducted several experiments on real images, which were taken using a SONY DXC-9000, a progressive 3 CCD digital camera, by setting its gamma correction off. To ensure that the outputs of the camera are linear to the flux of incident light, we used a spectrometer: Photo Research PR-650. We examined the algorithm using four types of input, i.e., uniform colored surfaces, multicolored surfaces, highly textured surfaces, and a scene multiple objects. We used convex objects to avoid interreflection, and excluded saturated pixels from the computation. For evaluation, we compared the results with the average values of image chromaticity of a white reference image (Photo Research Reflectance Standard model SRS-3), captured by the same camera. The standard deviations of these average values under various illuminant positions and colors were approximately $0.01 \sim 0.03$.

5.1 Color Constancy

Result on a uniformly colored surface Figure 15.a shows a real image of a head model that has a uniformly colored surface and relatively low specularity, illuminated by Solux Halogen with temperature $4700K$. Under the illumination, the image chromaticity of the white reference taken by our camera has chromaticity value: $\Gamma_r = 0.371, \Gamma_g = 0.318, \Gamma_b = 0.310$.

Figure 15.b shows the specular points of the red channel of chromaticity in inverse-intensity chromaticity space. Even though there is some noise, generally, all points form several straight lines heading for a certain point in the chromaticity axis. The same phenomenon can also be observed in Figure 15.c and Figure 15.d. Figure 16 shows the intersection-counting distribution in the illumination-chromaticity count space. The peaks of the distribution denote the illumination chromaticity. The result of the estimation was: $\Gamma_r = 0.378, \Gamma_g = 0.324, \Gamma_b = 0.287$.

Result on a multi-colored surface Figure 17.a shows a plastic toy with a multicolored surface. The illumination is Solux Halogen covered with a green filter. The image chromaticity of the white reference under this illuminant taken by our camera was $\Gamma_r = 0.298, \Gamma_g = 0.458, \Gamma_b = 0.244$.

Figure 17.b, c, d show the specular points of multiple surface colors in inverse-intensity chromaticity space. From Figure 18, we can observe that, even for several surface colors, the peak of intersection counts was still at a single value of Γ_c. The result of the estimation was $\Gamma_r = 0.319, \Gamma_g = 0.439, \Gamma_b = 0.212$.

Result on highly textured surface Figure 19.a shows a magazine cover with a complex multicolored surface, which was lit by a fluorescent light covered with a green filter. The image chromaticity of the white reference under this illuminant taken by our camera has a chromaticity value of $\Gamma_r = 0.283, \Gamma_g = 0.481, \Gamma_b = 0.236$. The result of the estimation was $\Gamma_r = 0.315, \Gamma_g = 0.515, \Gamma_b = 0.207$, as shown in Figure 20.

Result on multiple objects Figure 21.a shows a scene with multiple objects, which was lit by a fluorescent light taken in uncontrolled environment. The image chromaticity of the white reference under this illuminant taken by our camera has a chromaticity value of $\Gamma_r = 0.337, \Gamma_g = 0.341, \Gamma_b = 0.312$. The result of the estimation was $\Gamma_r = 0.321, \Gamma_g = 0.346, \Gamma_b = 0.309$, as shown in Figure 22.

Evaluation To evaluate the robustness of our method, we have also conducted experiments on 6 different objects: 2 objects with a single surface color, 1 object with multiple surface colors, and 3 objects with highly textured surfaces. The colors of illuminants were grouped into 5 different colors: Solux Halogen lamp with temperature $4700K$, incandescent lamp with temperature around $2800K$, Solux Halogen lamp covered with green, blue and purple filters. The illuminants were arranged at various positions. The total of images in our experiment was 43 images. From these images, we calculated the errors of the estimation by comparing them with the image chromaticity of the white reference, which are shown in Table 1. The errors are considerably small, as the standard deviations of the reference image chromaticity are around $0.01 \sim 0.03$.

Table 1: The performance of the estimation method with regard to the image chromaticity of the white reference

	red	green	blue
average of error	0.0172	0.0141	0.0201
std. dev. of error	0.01	0.01	0.01

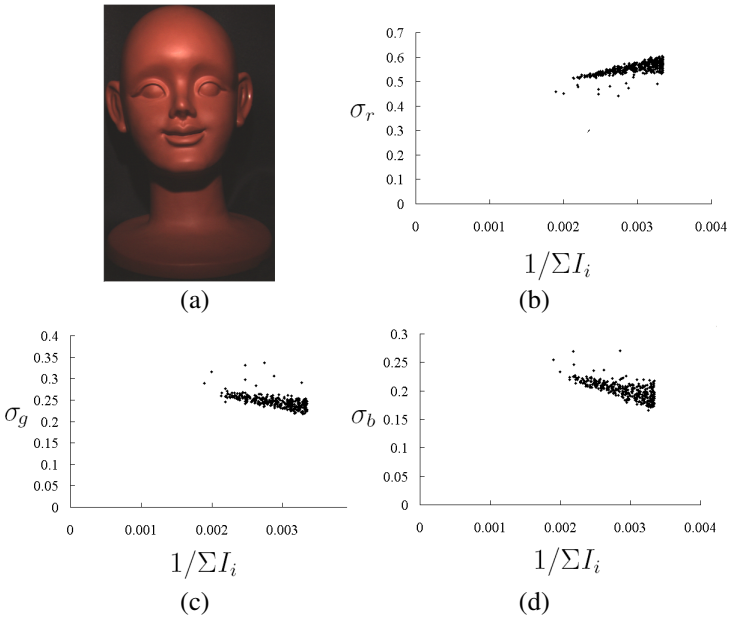

Figure 15: (a) Real input image with a single surface color. (b) Projection of the red channel of the specular pixels into inverse-intensity chromaticity space. (c) Projection of the green channel of the specular pixels into inverse-intensity chromaticity space. (d) Projection of the blue channel of the specular pixels into inverse-intensity chromaticity space.

5.2 Reflection Components Separation

We evaluate the separation results by comparing the results of two polarizing filters. We place one of the two filters in front of camera and the other in front of the light source. Theoretically, if we change the polarization angle of one of the two filters into a certain angle, we can obtain diffuse only reflection. In our experiment, we changed the polarization angle of the filter placed in front of the camera. Figure 5.2.a, b and c show, respectively, the input image, the diffuse reflection component obtained using the two polarizing filters (ground truth) and reflection components estimated using our method. Figure 5.2.d, e and f show the difference of image intensity values of the input image (Figure 5.2.a) and the ground truth (Figure 5.2.b), in red, green and blue channels, respectively. The ranges of blue pixels in the figures are $0 \sim 5$. Green pixels are $6 \sim 15$, red pixels are $16 \sim 35$, while yellow pixels represent larger than 35. In highlighted regions, we can observe a large difference of the intensity values in all color channels. Also, in certain places near occluding boundaries, yellow and red pixels also appear; this is caused by the difference of intensity distribution when the polarization angle is changed. Figure 5.2.g, h and i show the difference of image intensity values of the estimated reflection component (Figure 5.2.c) and the ground truth (Figure 5.2.b) in red, green and blue, respectively. In former highlighted regions, the colors became blue, indicating that the estimation result was considerably accurate. Red and green pixels occurring in many places in the comparison are due to two main factors: inaccurate illumination chromaticity estimation, and the second type of noise (dark noise) that occurs as the result of using polarizing filters. Despite these factors, the estimation results are considerably accurate, since the maximum value of second type of noise of the camera (Sony DXC-9000) is around 10. Figure 5.10 shows another separation result using a different object. Note that, in this evaluation, we do not evaluate pixels whose image intensity below camera is dark (black pixels in the evaluation represent unevaluated parts).

For a complex textured surface, Figure 24.a shows an image of a textured surface under fluorescent lights in uncontrolled environment. The specular-free image, which was generated by

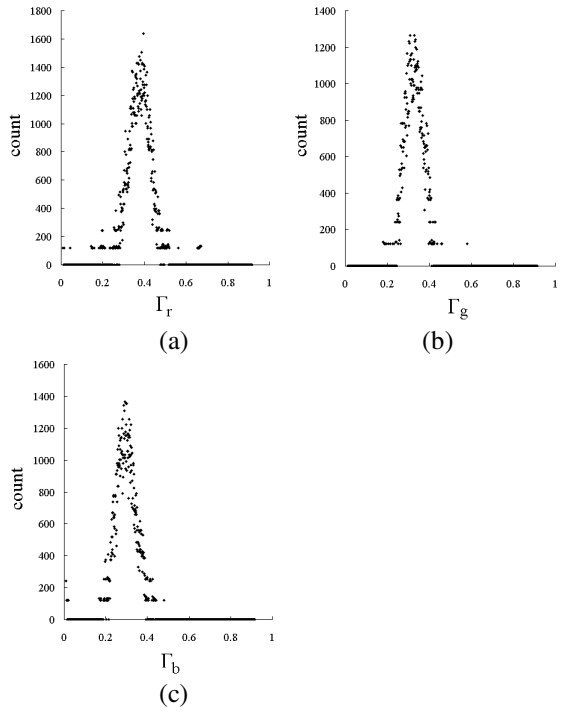

Figure 16: (a) Intersection-counting distribution for red channel of illumination chromaticity for image in Figure 15. (b) Intersection-counting distribution for green-channel. (c) Intersection-counting distribution for blue channel.

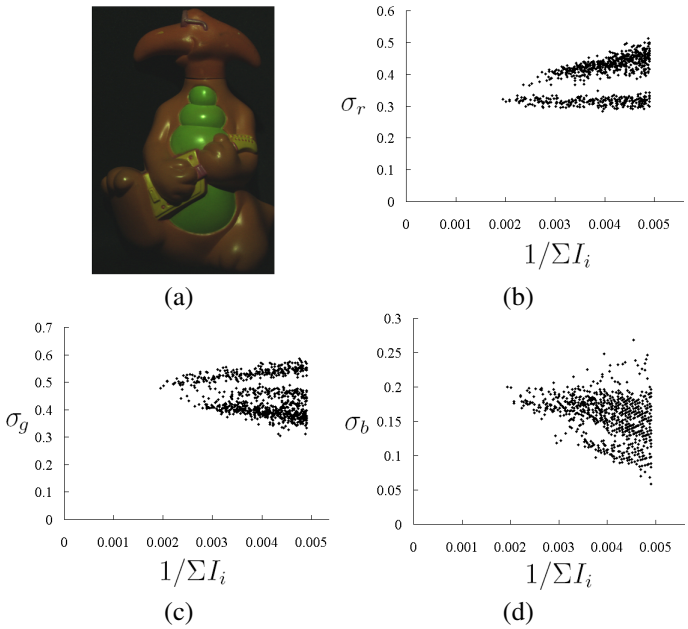

Figure 17: (a) Real input image with multiple surface colors. (b) Projection of the red channel of the specular pixels into inverse-intensity chromaticity space. (c) Projection of the green channel of the specular pixels into inverse-intensity chromaticity space. (d) Projection of the blue channel of the specular pixels into inverse-intensity chromaticity space.

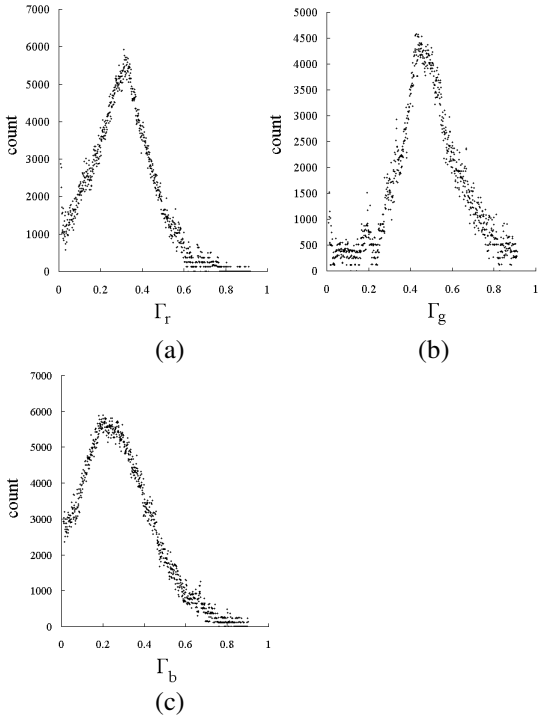

Figure 18: (a) Intersection-counting distribution for the red channel of illumination chromaticity for image in Figure 17. (b) Intersection-counting distribution for the green channel. (c) Intersection-counting distribution for the blue channel.

setting $\tilde{\Lambda}^{new}$ equal to 0.5 is shown in Figure 24.b. Figure 24.c and 24.d show the separated components of the object. Figure 27.a shows a complex scene lit with fluorescent lights in an uncontrolled environment. The specular-free image result is shown in Figure 27.b. Figure 27.c and Figure 27.d show the diffuse and specular reflections, respectively. In the estimated diffuse component (Figure 28.a) and the specular-free image (Figure 28.b), regions which are originally white become dark. The reason is that the specular-to-diffuse mechanism fails to handle achromatic pixels.

6 Conclusion

We have introduced a novel method for illumination chromaticity estimation. The proposed method can handle both uniform and non-uniform surface color objects. Given crude highlight regions, the method can estimate illumination color without requiring color segmentation. It is also applicable for multiple objects with various colored surfaces, as long as there are no interreflections. In this paper, we also introduced *inverse-intensity chromaticity space* to analyze the relationship between illumination chromaticity and image chromaticity. There are a few advantages of the method. First, the capability to cope with either single surface color or multiple surface colors. Second, color segmentation inside highlight regions and intrinsic camera characteristics are not required. Third, the method does not use strong constraints on illumination, which several existing color constancy methods use, such as blackbody radiator.

We also have proposed a novel method to separate diffuse and specular reflection components. The main insight of the method is on the chromaticity-based iteration with regard to the logarithmic differentiation of the specular-free image. Using the method, the separation problem in textured surfaces with complex multicolored scene can be resolved without requiring explicit color segmentation. It is possible because we base our method on local operation by utilizing the specular-free im-

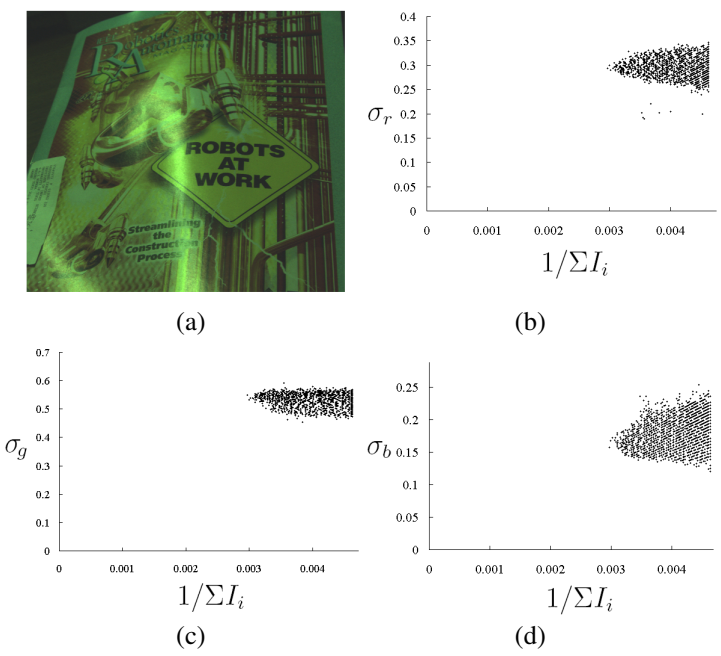

Figure 19: (a) Real input image of complex textured surface. (b) Projection of the red channel of the specular pixels into inverse-intensity chromaticity space. (c) Projection of the green channel of the specular pixels into inverse-intensity chromaticity space. (d) Projection of the blue channel of the specular pixels into inverse-intensity chromaticity space.

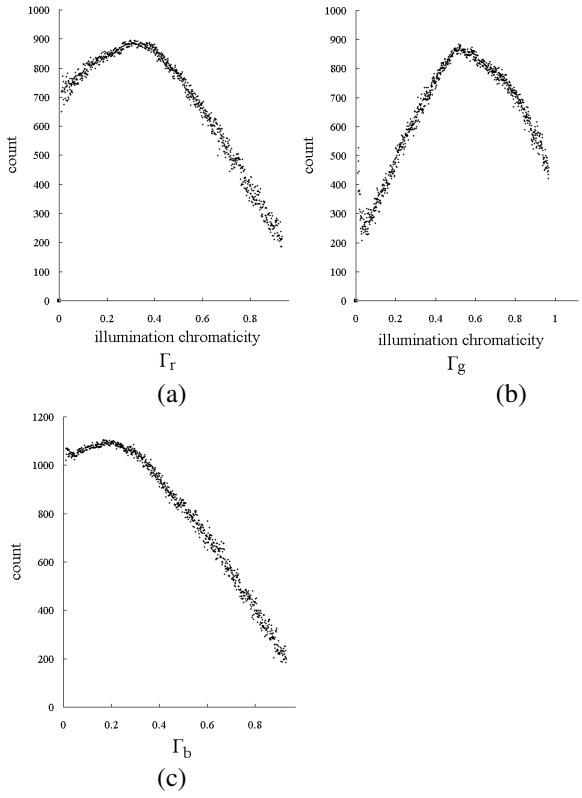

Figure 20: (a) Intersection-counting distribution for the red channel of illumination chromaticity for image in Figure 19. (b) Intersection-counting distribution for the green channel. (c) Intersection-counting distribution for the blue channel.

age. There are three crucial factors, and thus the main contributions of our method, i.e., the specular-to-diffuse mechanism, the specular-free image, and the logarithmic differentiation-based iteration framework.

The experimental results of our color constancy and reflection components separation on complex textured images show that the proposed methods are accurate and robust.

Acknowledgements

This research was, in part, supported by Japan Science and Technology (JST) under CREST Ikeuchi Project.

Appendix A

Derivation of the correlation between illumination chromaticity and image chromaticity.

$$\tilde{\sigma}'(\mathbf{x}) = \frac{m_d(\mathbf{x})\tilde{\Lambda}'(\mathbf{x}) + m_s(\mathbf{x})}{m_d(\mathbf{x})[\Lambda'_r(\mathbf{x}) + \Lambda'_g(\mathbf{x}) + \Lambda'_b(\mathbf{x})] + 3m_s(\mathbf{x})} \quad (37)$$

where $[\Lambda'_r + \Lambda'_g + \Lambda'_b] = 1$. For local (pixel based) operation the location $(\mathbf{x})$ can be removed. Then:

$$m_s = m_d \frac{(\tilde{\Lambda}' - \tilde{\sigma}')}{(3\tilde{\sigma}' - 1)} \quad (38)$$

Substituting m_s in the definition of $\tilde{I}$ (Equation (17)) with m_s in the last equation:

$$\tilde{I}' = m_d(\tilde{\Lambda}' - 1/3)(\frac{\tilde{\sigma}'}{\tilde{\sigma}' - 1/3}) \quad (39)$$

Appendix B

A diffuse pixel from a normalized image can be described as: $\mathbf{I}'(\mathbf{x}) = m_d(\mathbf{x})\mathbf{\Lambda}'(\mathbf{x})$. In Section 4.2, we have shown that using specular-to-diffuse mechanism by substituting $\tilde{\Lambda}'$ with an arbitrary value ($\tilde{\Lambda}^{new}$) whose value is between $1/3 \sim 1$, we can obtain:

$$\mathring{\mathbf{I}}(\mathbf{x}) = \mathring{m}_d(\mathbf{x})\mathring{\mathbf{\Lambda}}(\mathbf{x}) = m_d(\mathbf{x})k\mathring{\mathbf{\Lambda}}(\mathbf{x}) \quad (40)$$

where, for a pixel not located at color discontinuity, k is a constant scalar value ($k = \frac{3\tilde{\Lambda}'(\mathbf{x})-1}{3\tilde{\Lambda}^{new}-1}$).

A specular pixel with identical diffuse geometrical profile to the above diffuse pixel is described as: $\mathbf{I}'(\mathbf{x}) = m_d(\mathbf{x})\mathbf{\Lambda}'(\mathbf{x}) + m_s(\mathbf{x})$. By applying specular-to-diffuse mechanism to the specular pixel with the same value of $\tilde{\Lambda}^{new}$, we can obtain:

$$\mathring{m}_d(\mathbf{x}) = \frac{\tilde{I}'(\mathbf{x})[3\tilde{\sigma}'(\mathbf{x}) - 1]}{\tilde{\sigma}'(\mathbf{x})[3max(\tilde{\Lambda}^{new} - 1]} \quad (41)$$

where $\tilde{I}'(\mathbf{x}) = m_d(\mathbf{x})\tilde{\Lambda}'(\mathbf{x}) + m_s(\mathbf{x})$, and $\tilde{\Lambda}^{new}$ is the arbitrary maximum chromaticity. Unlike diffuse pixels, for specular pixels, $\tilde{\sigma}' \neq \tilde{\Lambda}'$. Then, the last equation becomes:

$$\mathring{m}_d(\mathbf{x}) = \Big[m_d(\mathbf{x})\tilde{\Lambda}'(\mathbf{x}) + m_s(\mathbf{x})\Big] \frac{[3\tilde{\sigma}'(\mathbf{x}) - 1]}{\tilde{\sigma}'(\mathbf{x})[3\tilde{\Lambda}^{new} - 1]} \quad (42)$$

Since we argued that in specular-free image specular reflection disappear ($\mathring{m}_s = 0$), then $\mathring{m}_d$ of the specular pixel should equal to $\mathring{m}_d$ of the diffuse pixel:

$$\mathring{m}_d^{diff} = \mathring{m}_d^{spec} \quad (43)$$

$$m_d\Big[\frac{3\tilde{\Lambda}'(\mathbf{x}) - 1}{3\tilde{\Lambda}^{new} - 1}\Big] = \Big[m_d(\mathbf{x})\tilde{\Lambda}'(\mathbf{x}) + m_s(\mathbf{x})\Big] \quad (44)$$

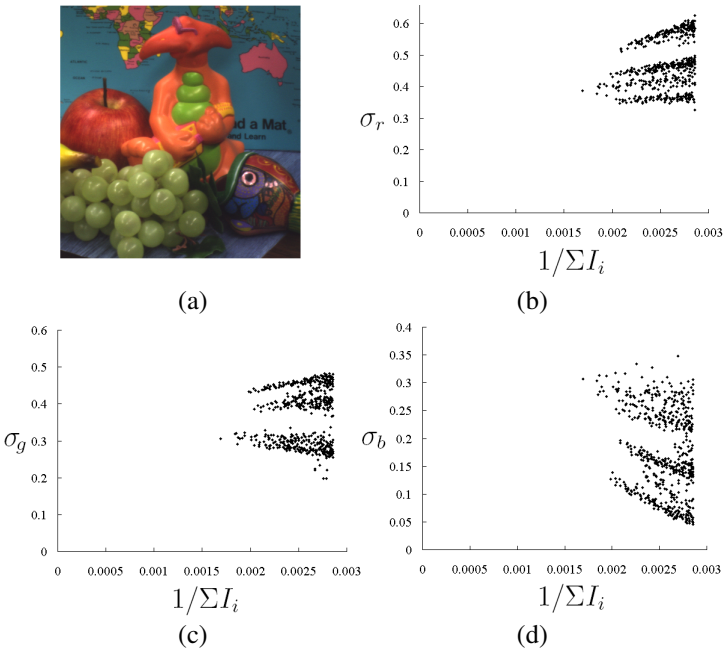

Figure 21: (a) Real input image of a scene with multiple objects. (b) Result of projecting the specular pixels into inverse-intensity chromaticity space, with c representing the red channel. (c) Result of projecting the specular pixels, with c representing the green channel. (d) Result of projecting the specular pixels, with c representing the blue channel.

$$\frac{[3\tilde{\sigma}'(\mathbf{x})-1]}{\tilde{\sigma}'(\mathbf{x})[3\tilde{\Lambda}^{new}-1]}$$

$$m_d(\mathbf{x})\Big[3\tilde{\Lambda}'(\mathbf{x})-1\Big]\tilde{\sigma}'(\mathbf{x}) = m_d(\mathbf{x})\tilde{\Lambda}'(\mathbf{x})\Big[3\tilde{\sigma}'(\mathbf{x})-1\Big] - m_s(\mathbf{x})\Big[3\tilde{\sigma}'(\mathbf{x})-1\Big] \quad (45)$$

$$m_d(\mathbf{x})\Big[\tilde{\Lambda}'(\mathbf{x})-\tilde{\sigma}'(\mathbf{x})\Big] = m_s(\mathbf{x})\Big[3\tilde{\sigma}'(\mathbf{x})-1\Big] \quad (46)$$

$$m_s(\mathbf{x}) = m_d(\mathbf{x})\frac{(\tilde{\Lambda}'(\mathbf{x})-\tilde{\sigma}'(\mathbf{x}))}{(3\tilde{\sigma}'(\mathbf{x})-1)} \quad (47)$$

the last equation is identical to Equation (38) in Appendix A, which proves that $\mathring{m}_d^{diff} = \mathring{m}_d^{spec}$ holds true. Therefore, all pixels in a specular-free image have no specular reflection component and its geometrical profile is identical to the diffuse component of the input image.

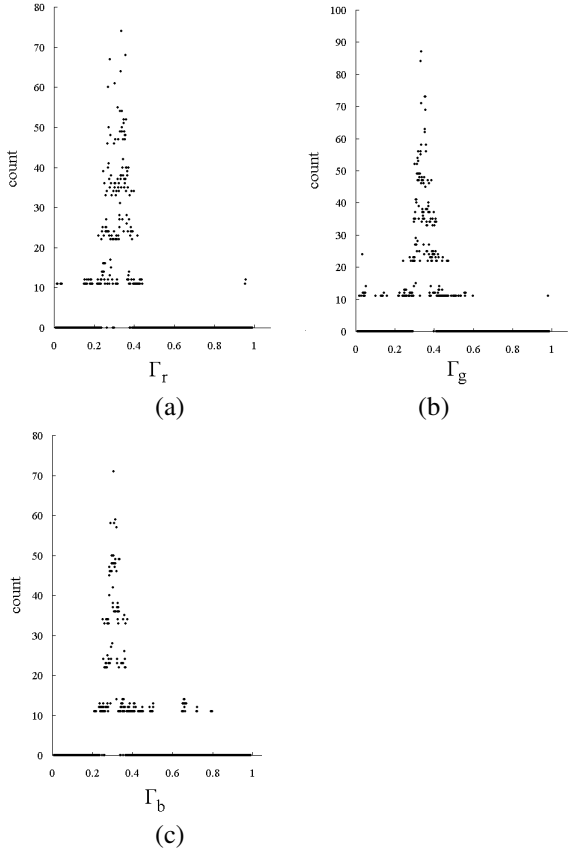

Figure 22: (a) Intersection-counting distribution for the red channel of illumination chromaticity for image in Figure 19. (b) Intersection-counting distribution for the green channel. (c) Intersection-counting distribution for the blue channel.

References

[1] H.J. Andersen and E. Granum. Classifying illumination conditions from two light sources by colour histogram assessment. *Journal of Optics Society of America A.*, 17(4):667–676, 2000.

[2] R. Bajscy, S.W. Lee, and A. Leonardis. Detection of diffuse and specular interface reflections by color image segmentation. *International Journal of Computer Vision*, 17(3):249–272, 1996.

[3] P. Beckmann and A. Spizzochino. *The scattering of electromagnetic waves from rough surfaces*. Pergamon, New York, 1963.

[4] D.H. Brainard and W.T. Freeman. Bayesian color constancy. *Journal of Optics Society of America A.*, 14(7):1393–1411, 1997.

[5] A. Criminisi, S.B. Kang, R. Swaminathan, S. Szeliski, and P. Anandan. Extracting layers and analysis their specular properties using epipolar plane image analysis. *Microsoft Research Technical Report MSR-TR-2002-19*, 2002.

[6] M. D'Zmura and P. Lennie. Mechanism of color constancy. *Journal of Optics Society of America A.*, 3(10):1162–1672, 1986.

[7] G.D. Finlayson. Color in perspective. *IEEE Trans. on Pattern Analysis and Machine Intelligence*, 18(10):1034–1038, 1996.

[8] G.D. Finlayson and B.V. Funt. Color constancy using shadows. *Perception*, 23:89–90, 1994.

[9] G.D. Finlayson, S.D. Hordley, and P.M. Hubel. Color by correlation: a simple, unifying, framework for color constancy. *IEEE Trans. on Pattern Analysis and Machine Intelligence*, 23(11):1209–1221, 2001.

[10] G.D. Finlayson and G. Schaefer. Convex and non-convex illumination constraints for dichromatic color constancy. In *in proceeding of IEEE Computer Society Conference on Computer Vision and Pattern Recognition (CVPR)*, volume I, page 598, 2001.

[11] G.D. Finlayson and G. Schaefer. Solving for color constancy using a constrained dichromatic reflection model. *International Journal of Computer Vision*, 42(3):127–144, 2001.

[12] G.D. Finlayson and S.D.Hordley. Color constancy at a pixel. *Journal of Optics Society of America A.*, 18(2):253–264, 2001.

[13] B.V. Funt, M. Drew, and M. Brockington. Recovering shading from color images. *in proceeding of European Conference on Computer Vision (ECCV)*, pages 124–132, 1992.

[14] B.V. Funt, M. Drew, and J. Ho. Color constancy from mutual reflection. *International Journal of Computer Vision*, 6(1):5–24, 1991.

[15] R. Gershon, A.D. Jepson, and J.K. Tsotsos. Ambient illumination and the determination of material changes. *Journal of Optics Society of America A.*, 3(10):1700–1707, 1986.

[16] J.M. Geusebroek, R. Boomgaard, S. Smeulders, and H. Geert. Color invariance. *IEEE Trans. on Pattern Analysis and Machine Intelligence*, 23(12):1338–1350, 2001.

[17] J.M. Geusebroek, R. Boomgaard, S. Smeulders, and T. Gevers. A physical basis for color constancy. In *The First European Conference on Colour in Graphics, Image and Vision*, pages 3–6, 2002.

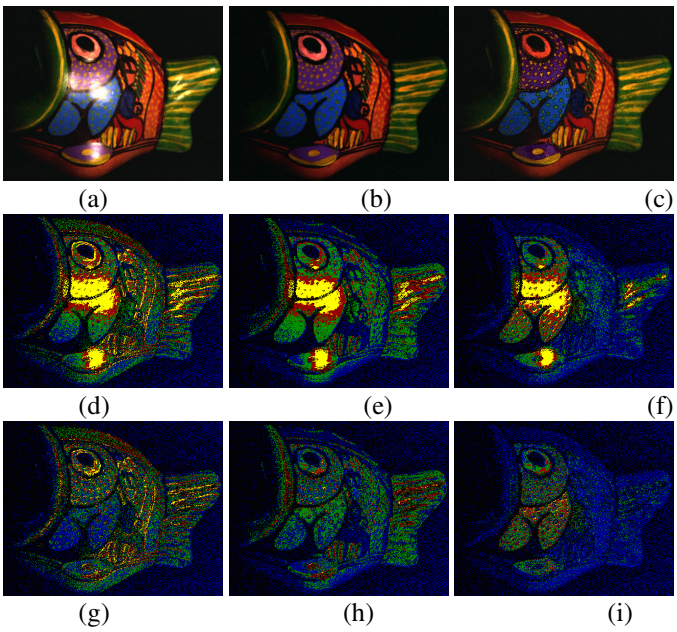

(a) (b) (c)

(d) (e) (f)

(g) (h) (i)

Figure 23: Top: (a) Textured input image (b) ground truth (c) estimation. Middle: specular-ground truth comparison: (d) R-channel (e) G-channel (f) B-channel. Bottom: error:(d) R-channel (e) G-channel (f) B-channel

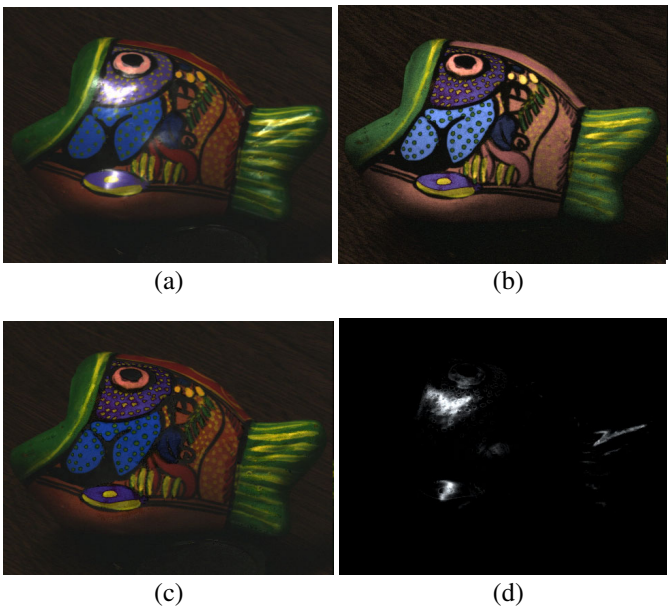

(a) (b)

(c) (d)

Figure 24: (a) A complex textured surface lit with fluorescent lights. (b) The specular-free image was created by setting $\tilde{\Lambda}' = 0.5$. (c) Diffuse reflection component. (d) Specular reflection component.

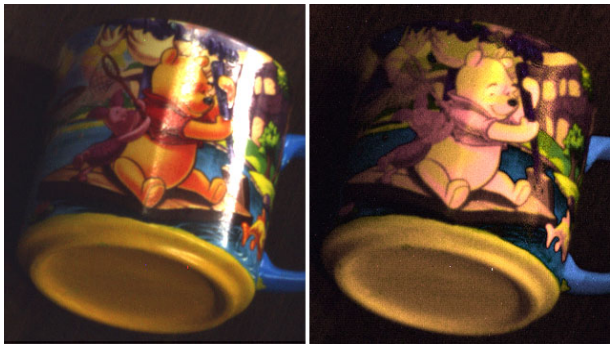

(a) (b)

Figure 25: (a) a complex textured surface of a cup lit with fluorescent lights (b) the specular-free image by setting $\tilde{\Lambda} = 0.5$

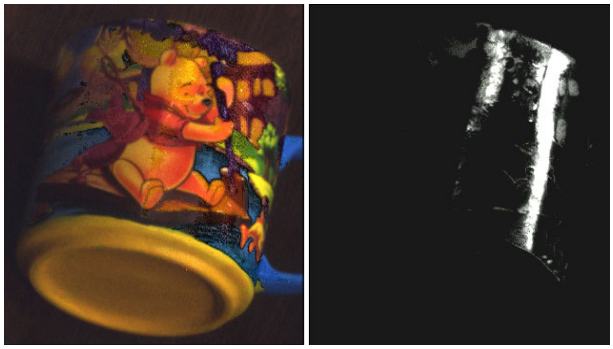

(a) (b)

Figure 26: (a) estimated diffuse reflection component (b) estimated specular reflection component.

[18] R.C. Gonzales and R.E. Woods. *Digital Image Processing*. Addison-Wesley, 1993.

[19] G. Healey and R. Kondepudy. Radiometric ccd camera calibration and noise estimation. *IEEE Trans. on Pattern Analysis and Machine Intelligence*, 16(3):267–276, 1994.

[20] J.M.Rubin and W.A.Richard. Color vision: representing material changes. *AI Memo 764, MIT Artificial Intelligence Lab. Cambridge, Mass.*, 1984.

[21] G.J. Klinker, S.A. Shafer, and T. Kanade. The measurement of highlights in color images. *International Journal of Computer Vision*, 2:7–32, 1990.

[22] J.H. Lambert. Photometria sive de mensura de gratibus luminis, colorum et umbrae. *Eberhard Klett: Augsberg, Germany*, 1760.

[23] H.C. Lee. Method for computing the scene-illuminant from specular highlights. *Journal of Optics Society of America A.*, 3(10):1694–1699, 1986.

[24] H.C. Lee. Illuminant color from shading. In *Perceiving, Measuring and Using Color*, page 1250, 1990.

[25] H.C. Lee, E.J. Breneman, and C.P.Schulte. Modeling light reflection for computer color vision. *IEEE Trans. on Pattern Analysis and Machine Intelligence*, 12:402–409, 1990.

[26] S.W. Lee. *Understanding of surface reflections in Computer vision by color and multiple views*. PhD thesis, University of Pennsylvania, 1991.

[27] S.W. Lee and R. Bajcsy. Detection of specularity using color and multiple views. *Image and Vision Computing*, 10:643–653, 1992.

[28] T.M. Lehmann and C. Palm. Color line search for illuminant estimation in real-world scene. *Journal of Optics Society of America A.*, 18(11):2679–2691, 2001.

[29] S. Lin, Y. Li, S.B. Kang, X. Tong, and H.Y. Shum. Diffuse-specular separation and depth recovery from image sequences.

Figure 27: (a) a complex multicolored scene lit with fluorescent lights (b) The specular-free image by setting $\tilde{\Lambda} = 0.5$

Figure 28: (a) Diffuse reflection component (b) Specular reflection component

In *in proceeding of European Conference on Computer Vision (ECCV)*, pages 210–224, 2002.

[30] S. Lin and H.Y. Shum. Separation of diffuse and specular reflection in color images. In *in proceeding of IEEE Computer Society Conference on Computer Vision and Pattern Recognition (CVPR)*, 2001.

[31] S.K. Nayar, X.S. Fang, and T. Boult. Separation of reflection components using color and polarization. *International Journal of Computer Vision*, 21(3), 1996.

[32] S.K. Nayar, K.Ikeuchi, and T. Kanade. Surface reflection: Physical and geometrical perspectives. *IEEE Trans. on Pattern Analysis and Machine Intelligence*, 13(7):611–634, 1991.

[33] J.P.S. Parkkinen, J. Hallikainen, and T. Jasskelainen. Characteristic spectra of munsell colors. *Journal of Optics Society of America A.*, 6, 1989.

[34] C. Rosenberg, M. Hebert, and S. Thrun. Color constancy using kl-divergence. In *in proceeding of IEEE International Conference on Computer Vision (ICCV)*, volume I, page 239, 2001.

[35] Y. Sato and K. Ikeuchi. Temporal-color space analysis of reflection. *Journal of Optics Society of America A.*, 11, 1994.

[36] S. Shafer. Using color to separate reflection components. *Color Research and Applications*, 10:210–218, 1985.

[37] R. T. Tan and K. Ikeuchi. Separating reflection components of textured surfaces using a single image. *in proceeding of IEEE International Conference on Computer Vision (ICCV)*, pages 870–877, 2003.

[38] R. T. Tan, K. Nishino, and K. Ikeuchi. Illumination chromaticity estimation using inverse-intensity chromaticity space. *in proceeding of IEEE Computer Society Conference on Computer Vision and Pattern Recognition (CVPR)*, pages 673–680, 2003.

[39] R. T. Tan, K. Nishino, and K. Ikeuchi. Reflection components separation based-on chromaticity and noise analysis. *in proceeding of IEEE International Workshop on Color and Photometric Methods in Computer Vision (CPMCV)*, 2003.

[40] R. T. Tan, K. Nishino, and K. Ikeuchi. Color constancy through inverse intensity chromaticity space. *Journal of Optics Society of America A.*, 21(3):321–334, 2004.

[41] R. T. Tan, K. Nishino, and K. Ikeuchi. Separating reflection components based on chromaticity and noise analysis. *IEEE Trans. on Pattern Analysis and Machine Intelligence*, to appear, 2004.

[42] S. Tominaga. A multi-channel vision system for estimating surface and illumination functions. *Journal of Optics Society of America A.*, 13(11):2163–2173, 1996.

[43] S. Tominaga, S. Ebisui, and B.A. Wandell. Scene illuminant classification: brighter is better. *Journal of Optics Society of America A.*, 18(1):55–64, 2001.

[44] S. Tominaga and B.A. Wandell. Standard surface-reflectance model and illumination estimation. *Journal of Optics Society of America A.*, 6(4):576–584, 1989.

[45] S. Tominaga and B.A. Wandell. Natural scene-illuminant estimation using the sensor correlation. *Proceedings of the IEEE*, 90(1):42–56, 2002.

[46] K.E. Torrance and E.M. Sparrow. Theory for off-specular reflection from roughened surfaces. *Journal of Optics Society of America*, 57:1105–1114, 1966.

[47] L.B. Wolff and T. Boult. Constraining object features using polarization reflectance model. *IEEE Trans. on Pattern Analysis and Machine Intelligence*, 13(7):635–657, 1991.